Iranian Journal of Geophysics, Vol 21 No 3, 2027, Page 1 – 26 (Research Article)
DOI: 10.30499/ijg.2026.547572.1726

A pattern recognition approach to reservoir modeling: comparative performance of CNN and gradient boosting in heterogeneous carbonate reservoirs

Yeganeh Mirakhorloo [1], Forough Zaker Moshfegh [2]and Reza Hoveyzavi [3*]

[1] *M.Sc., Department of Artificial Intelligence, Asmary Field Services Company, Tehran, Iran*
[2] *M.Sc., Department of Artificial Intelligence, Asmary Field Services Company, Tehran, Iran*
[3] *Ph.D., Department of Training, Asmary Field Services Company, Tehran, Iran*

(Received: 21 September 2025, Accepted: 02 April 2026)

Abstract

Missing intervals or unreliable well-log measurements pose a persistent challenge for subsurface characterization, particularly for curves critical to porosity, lithology, and velocity analysis. This study investigates two machine-learning strategies for reconstructing missing logs: a hybrid Multivariate Imputation by Chained Equations with Gradient Boosted Trees (MICE+GBT), and also Convolutional Neural Network (CNN). The prediction targets are three essential logs-neutron porosity (NPHI), bulk density (RHOB), and compressional travel time (DT). Each reconstructed artificial log from complementary measurements including resistivity, Photoelectric Factor (PEF), and spectral gamma-ray. A rigorous preprocessing workflow was applied, followed by evaluation under a well-level cross-validation scheme to simulate deployment on unseen wells. Performance was measured using Mean Squared Error (MSE), Mean Absolute Error (MAE), correlation coefficient (R), and coefficient of determination (R^2). This research utilizes two separate methods to estimate absent well logs in the Sarvak Formation, a diverse carbonate reservoir noted for intricate pore configurations and variability in lithology. These approaches tackle deficiencies in log data while assessing performance in regulated environments. In the following section, we will outline the dataset, prediction objectives, preprocessing steps, workflows, and evaluation methods. Results indicate that the MICE+GBT approach consistently outperforms Convolutional LSTM across all three target logs, particularly for intervals affected by washouts or tool measurement failures. Beyond statistical performance, the reconstructed curves preserved geological consistency in density–neutron and sonic–density trends, ensuring reliability for downstream reservoir interpretation. The findings demonstrate the practical benefits of adapting ensemble-based imputation methods to petrophysical data, providing a robust and interpretable framework for improving log data alliance in reservoir studies. Results demonstrated that the MICE+GBT workflow consistently delivered accurate, stable, and interpretable predictions across both Danan and Azadegan fields. Its strength was most evident in DT reconstruction, where ConvLSTM struggled with convergence and produced elevated error magnitudes. Ensemble models also yielded narrower error distributions and superior generalization across wells, underscoring their robustness in data-limited carbonate environments. Conversely, the ConvLSTM framework captured local depth-wise dependencies effectively, particularly for NPHI, and showed potential when sufficient training data were available. However, its sensitivity to heterogeneity and tendency toward error dispersion limit its reliability in reservoirs with strong lithological variability. Overall, the findings suggest that ensemble methods presently offer more dependable solutions for carbonate reservoirs with restricted datasets, while deep learning approaches hold promise for future applications given larger, more diverse training corpora. Integrating the interpretability and stability of ensemble models with the representational power of deep learning could form the basis of next-generation workflows for missing log prediction.

Keywords: Gradient boosting tree(GBT), petrophysical Well Logs, conventional long short-term memory (CONVLSTM), convolutional nerural network (CNN), machine learning (ML)

*Corresponding author: Hoveyzavi@asmaryco.com

1 Introduction

Petrophysical well logs are fundamental tools for subsurface characterization, essential for reservoir evaluation, petrophysical property determination, and decision-making in hydrocarbon exploration and production. These logs yield critical data on porosity, lithology, fluid saturation, and other reservoir attributes. However, field operations often result in gaps or missing intervals due to borehole instability, tool malfunctions, washouts, or cost-driven acquisition choices. Such omissions introduce substantial uncertainty, impairing workflows like porosity estimation, facies classification, and seismic calibration. Re-logging is typically impractical owing to high costs and risks associated with re-entering inaccessible wellbores. Consequently, developing efficient, reliable methods for reconstructing missing logs is a pressing concern in both academic research and industry practice (Wenyi and Horn, 2024; Artun, et al., 2025; Mukherjee, et al., 2024) .

Among petrophysical well logs, neutron porosity (NPHI), bulk density (RHOB), and compressional sonic travel time (DT) are particularly vital for reservoir characterization, as they underpin porosity calculations, lithology interpretation, and velocity modeling. Their absence poses significant hurdles in downstream analysis. Thus, accurate prediction of these logs has attracted considerable attention from researchers and practitioners (Al-Mudhafar, et al., 2025; Maldonado-Cruz, et al., 2023).

Over time, diverse approaches have addressed missing log prediction. Early methods employed empirical models, such as Gardner's velocity-density relation and Castagna's velocity transforms. While effective in specific lithologies, these required expert calibration and lacked flexibility for complex reservoirs (Gardner, et al., 1974; Castagna, et al., 1985). More recently, data-driven techniques have surged, with machine learning (ML) methods like linear regression, random forests, and artificial neural networks excelling at capturing non-linear relationships. Ensemble methods, notably Gradient Boosting, have proven robust for gap-filling (Lopes and Alípio, 2018).

Deep learning advancements have further transformed the field. Recurrent Neural Networks (RNNs) and Long Short-Term Memory (LSTM) networks effectively model sequential depth dependencies (Pham and Zabihi, 2019). Hybrid architectures, such as Convolutional Neural Networks (CNNs) integrated with LSTMs (CNN-LSTM) or Bidirectional LSTMs (BiLSTM) with attention mechanisms, capture local features and long-range patterns in log data (Shan Liqun, et al., 2021). Transformer-based models, leveraging self-attention for global dependencies, offer enhanced efficiency and accuracy (Lin Lei, et al. 2023).

Despite these strides, challenges endure in heterogeneous carbonate reservoirs, where intricate pore structures, diagenetic alterations, and lithological variability (e.g., vuggy porosity and dolomitization) complicate predictions (Al-Mudhafar, et al., 2025; Lin, Lei, et al. 2024). Robust, flexible models for such settings remain under development. Moreover, while DL studies abound, comparative evaluations of statistical-ensemble versus DL methods are scarce, particularly in carbonate contexts like the Middle East's reservoirs.

This study tackles missing log prediction from the Sarvak Formation, a Creta-

ceous carbonate reservoir in Iran's Zagros Fold-Thrust Belt known for its heterogeneity and secondary porosity. We employ two strategies:

- A statistical-ensemble approach, integrating Multivariate Imputation by Chained Equations (MICE) with Gradient Boosted Trees (GBT), building on prior elastic log reconstruction work.
- A DL-based approach using Convolutional LSTM models to capture non-linear depth dependencies and inter-log interactions.

Both are assessed via cross-validation and partial-missingness simulations to mimic real-world scenarios. Key contributions include:

- Application of MICE+GBT and Convolutional LSTM to predict NPHI, RHOB, and DT in the Sarvak Formation.
- Comparative analysis of ensemble versus DL methods across missingness patterns.
- Workflows emphasizing interpretability, robustness, and adaptability for practical reservoir applications.

This research offers insights into these techniques' performance in carbonate reservoirs, advancing reliable well log prediction at petroleum industry.

2 Theory

The reconstruction of missing well logs remains a persistent challenge in the petroleum industry, prompting the development of diverse methods ranging from empirical correlations to advanced ML and DL architectures. This section reviews key approaches in the literature, delineating their strengths and limitations, and identifies research gaps that this study addresses.

2.1.1 Empirical and Statistical Approaches

Early well log prediction relied on empirical methods, such as Gardner's velocity-density relationship. and Castagna's mud rock line for velocity transforms (Gardner, et al., 1974; Castagna, et al., 1985). These models leverage observed correlations between parameters like sonic velocity and density, offering quick estimates in uniform lithologies. Their strengths include simplicity and low computational demands, but they require site-specific calibration and falter in heterogeneous reservoirs where lithological variations (e.g., diagenetic effects in carbonates) disrupt assumed relationships. Subsequent statistical methods, including linear and multivariate regression, as well as interpolation techniques, enhanced flexibility by modeling multiple variables. For instance, kriging-based interpolation has been used for spatial gap-filling (Wenyi and Horn, 2024; Kiss and Norbert, 2022). However, these approaches often underperform in non-linear scenarios influenced by geophysical factors, failing to capture sequential depth dependencies critical for accurate predictions. In carbonates, where pore complexity amplifies variability, error rates can exceed 20% without additional constraints.

2.1.2 Machine Learning Methods

The advent of ML has shifted focus to data-driven models, including k-nearest neighbors (KNN), support vector machines (SVM), random forests, and gradient boosting machines (GBM). These excel at discerning non-linear patterns, improving accuracy in heterogeneous settings where empirical methods fail—for example, GBM variants like XGBoost have reduced prediction errors by 15-30% in clastic reservoirs. Ensemble methods, particularly GBM and

LightGBM, stand out for their robustness in handling high-dimensional data and minimizing bias/variance through iterative tree building(Lopes and Alípio, 2018). Comparative analyses indicate they outperform linear regression in generalization, especially with noisy datasets. Enhancements via feature engineering—incorporating lithology or seismic attributes—and hybrid imputation (e.g., with multivariate techniques) further boost performance (Alimohammadi, et al. 2020). Nonetheless, ML models can overfit without sufficient data and struggle with long-range sequential dependencies in depth-series logs (Mukherjee, et al., 2024; (Al-Mudhafar, et al., 2025).

2.1.3 Deep Learning Approaches

DL has revolutionized well log prediction by addressing sequential and spatial complexities. RNNs and LSTMs model depth-wise dependencies effectively, with demonstrated success in gap-filling sonic logs(Pham and Zabihi, 2019; Kanfar, et al., 2020). CNN-LSTM and BiLSTM hybrids extend this further, enhancing reconstruction in multi-log scenarios(Shan Liqun, et al., 2021). Attention-based models amplify accuracy gains in heterogeneous formations.

Applications include carbonate-specific workflows (Lin, Lei, et al. 2024) and uncertainty-aware frameworks for sonic logs (Maldonado-Cruz, et al., 2023). While powerful, DL models demand large datasets and computational resources, with risks of overfitting in data-scarce carbonate environments.

2.1.4 Attention-Based and Transformer Models

Emerging attention and transformer models offer efficient alternatives for long-range dependency modeling. Adapted from natural language processing, transformers process data in parallel, outperforming RNNs in scalability for large well log datasets. Frameworks like the Transformer-based Missing Well Log Prediction (MWLT) have demonstrated superior accuracy (e.g., 8-15% RMSE improvement over LSTMs) in capturing global contexts, especially in carbonates with variable porosity.

Their parallelization reduces training time, making them suitable for real-time applications. However, transformers can be data-hungry and less interpretable than simpler models, with limited testing in extreme missingness cases.

2.1.5 Research Gaps

Despite these advancements, notable gaps persist. First, most studies evaluate methods in isolation (e.g., solely DL or ML), lacking comprehensive cross-comparisons between statistical-ensemble and DL approaches (Wenyi and Horn, 2024; Artun, et al., 2025). Second, research on heterogeneous carbonate reservoirs is underrepresented, with fewer than 20% of publications addressing their unique challenges, such as vuggy porosity and diagenesis (Al-Mudhafar, et al., 2025). Third, evaluations under varied missingness scenarios (e.g., partial gaps vs. extended intervals) are scarce, limiting insights into practical robustness.

This study bridges these gaps by comparatively analyzing ensemble-based (MICE+GBT) and DL (Convolutional LSTM) methods for predicting NPHI, RHOB, and DT in the Sarvak Formation—a heterogeneous carbonate reservoir. By simulating real-world missingness and emphasizing carbonate complexities, we aim to advance reliable, adaptable workflows for subsurface characterization.

3 Methodology

This study employs two distinct approaches to predict missing well logs in the Sarvak Formation, a heterogeneous carbonate reservoir characterized by complex pore structures and lithological variability. These methodologies address gaps in log data while evaluating performance under controlled scenarios. At the below section, we will describe the dataset, prediction targets, preprocessing, workflows, and evaluation protocols.

Although this study does not introduce a new predictive model, it contributes scientifically by establishing a carbonate-specific evaluation and diagnostic framework that is absent in prior literature. The framework integrates multiple components that together form a novel benchmark for reconstructing missing logs in heterogeneous carbonate reservoirs:

1 Well-level Leave-One-Out Cross-Validation (LOOCV) applied separately in Danan and Azadegan fields to quantify intra-field generalization under complex lithologies.

2 Realistic missingness simulation, mimicking operational logging gaps and enabling controlled assessment of robustness.

3 Multi-target evaluation covering RHOB, NPHI, and DT simultaneously to capture target-specific sensitivities.

4 Uncertainty quantification for both ensemble and DL models, enabling evaluation beyond point accuracy.

5 Learning-curve-based diagnostic analysis, providing insights into why ConvLSTM underperforms on DT in carbonates.

6 Cross-field robustness testing, evaluating model transferability across two carbonate reservoirs with distinct heterogeneity levels.

Together, these elements form a reproducible benchmark framework tailored to carbonate formations, offering insights beyond conventional comparative studies and enabling standardized future research. Finally, to enhance interpretability and diagnose model-specific behavior, feature-importance analysis was incorporated to explain performance disparities between ensemble and deep learning approaches.

Data Preparation of the Appropriate Inputs

3.1 Data set and Prediction Targets

The dataset comprises well log data from 20 wells across two carbonate fields in the Sarvak Formation: Including Danan field (10 wells) and Azadehgan North field (10 wells). To simulate realistic conditions and assess intra-field generalizability, training and testing were conducted independently within each field (e.g., using 9 wells for training and 1 for testing in Danan). Seven primary logs were available consistently: gamma ray (GR), corrected gamma ray (CGR), compressional sonic travel time (DT), bulk density (RHOB), neutron porosity (NPHI), photoelectric factor (PEF), and deep resistivity (RD). Three auxiliary logs caliper (CALI), bit size (BI), and density correction (DRHO) supported preprocessing for washout detection but were excluded from modeling to focus on petrophysical predictors. The reconstruction process targeted three porosity-related logs: RHOB, NPHI, and DT, essential for reservoir evaluation in carbonates. In experiments, one target was randomly masked, with predictions derived from the remaining six logs as inputs. This setup enabled systematic assessment across targets, with datasets totaling ~100,000-130,000 depth samples after preprocessing across all the studied

wells.

3.2 Pre-processing

A two-stage preprocessing pipeline ensured data quality and model readiness. First, washout intervals—common in unstable carbonate boreholes were identified and removed using thresholds: CALI - BI > 2 inches for borehole enlargement and |DRHO| > 0.15 g/cm³ for density anomalies. These flagged intervals (~5-15% of data) were treated as missing to prevent biasing predictions.

Second, log-specific range conditioning filtered implausible values based on physical constraints: DT (40-160 μs/ft), RHOB (1.95-3.2 g/cm³), NPHI (-0.05-0.50 v/v), PEF (0-6 b/e), CGR (0-150 API), and RD (transformed to $\log_{10}$ scale for skewness reduction, clipped to realistic ranges). Outliers (~2-5% per log) were flagged as missing for imputation. Features were normalized using a standard scaler to equalize scales and stabilize training. Derived features (e.g., GR-derived lithology indicators) were added to enhance multivariate dependencies, leveraging domain knowledge for better prediction in heterogeneous reservoir settings.

3.3 MICE + GBT Workflow

The statistical-ensemble approach combined MICE with GBT for robust, interpretable imputation, adapted from elastic log reconstruction studies. MICE iteratively impute missing values by modeling each variable conditionally on others, generating multiple datasets for uncertainty estimation. We used LightGBM as the regressor for its efficiency in handling non-linear relationships and large datasets. Parameters included num of leaves=100 (for tree complexity), max depth=5 (to prevent overfitting), and random state=456 (for reproducibility). Imputation ran for 200 iterations chosen empirically for convergence in similar geophysical tasks with ascending variable order, mean initialization, and a tolerance of 0.001. This setup captured non-linear log interactions effectively, with GBT's ensemble nature reducing variance in carbonate data. Data splits used 9 wells per field for training (~90% of samples) and 1 for testing (~10%), ensuring out-of-sample evaluation.

3.4 MICE + GBT Architecture

The MICE+GBT workflow implemented in this study follows the structure originally introduced by (Hallam, et al., 2022). The process includes:
(1) missingness detection and masking,
(2) iterative imputation of missing logs using Multiple Imputation by Chained Equations (MICE), and
(3) boosted-tree prediction on the completed dataset.
To ensure reproducibility, the key hyperparameters used in this work are reported as:

- n_estimators = 500
- max_depth = 6
- learning_rate = 0.05
- subsample = 0.8
- loss = squared error

Hyperparameters were refined using cross-validated tuning consistent with the Hallam et al. framework. A schematic overview of the MICE-assisted GBT workflow is provided in Figure 1.

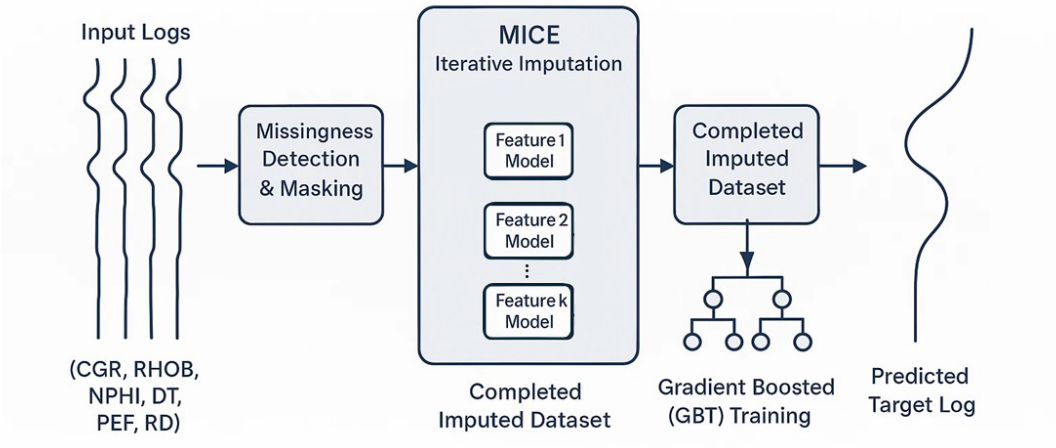

Figure 1. MICE+GBT architecture.

3.5 Convolutional LSTM Workflow

The deep learning approach utilized a ConvLSTM network to model local spatial features and long-range depth dependencies, ideal for sequential well log data in complex reservoirs.

The architecture included:

- Two ConvLSTM layers (16 and 128 units) for feature extraction and temporal modeling, with 1D convolutions (kernel size=3) to capture local patterns.
- Two fully connected layers (128 and 64 neurons) with ReLU activation, culminating in a single output neuron for regression.

Inputs were shaped as sequences (e.g., [batch size, depth steps, features=6]), outputting predicted targets. Training employed the Adam optimizer over 40 epochs (selected via early stopping) with batch size=32. Splits per field used 9 wells for training, leave one out cross-validation approach (hyperparameter tuning), and one for testing, keeping test data unseen to evaluate generalization.

3.6 ConvLSTM Architecture

The ConvLSTM framework employed in this study follows a standard sequence-modeling architecture widely used in well-log prediction tasks and is consistent with the baseline structures described by (Mukherjee, et al., 2024). Input logs were organized into sliding windows of 20 depth steps to preserve local sequential structure.

The network comprises two stacked ConvLSTM layers with 16 and 128 filters respectively (kernel size: 3×3), followed by a Flatten layer and two fully connected layers with 128 and 64 nodes. Standard LSTM gate activations are used within the recurrent blocks, while ReLU activation is applied in the dense layers. Model training utilized the Adam optimizer with a learning rate of 0.001. Early stopping (patience = 10) was applied with a maximum of 40 epochs, using MSE as the loss function.

This architecture enables the model to capture both spatial texture and sequential variability within heterogeneous carbonate intervals. The overall architecture of the ConvLSTM framework is illustrated in Figure 2.

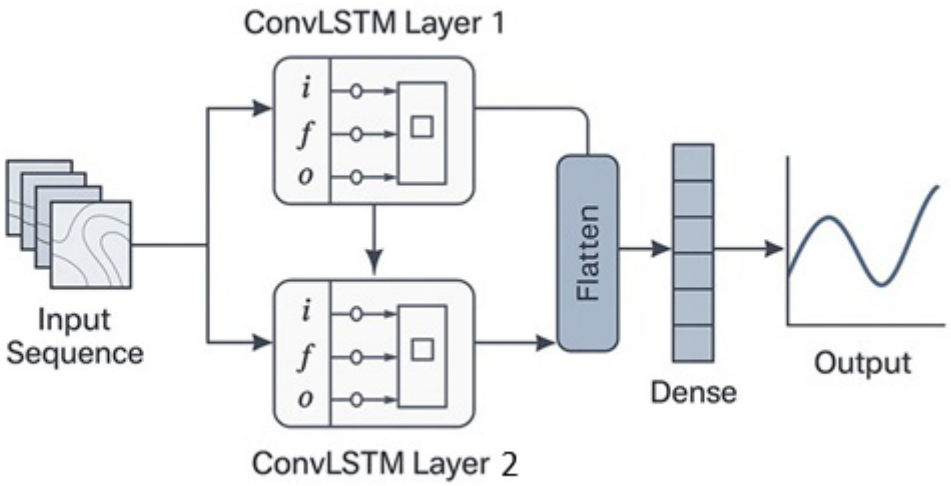

Figure 2. ConvLSTM architecture.

3.7 Evaluation Protocol

Performance was quantified using MSE, MAE, R, and R^2, assessing accuracy and fit. Robustness test by applying field-based tests by training on 9 wells and testing on 1 held-out well per field, mimicking new-well predictions in similar geology.

To ensure methodological reproducibility and a fair performance comparison between the two frameworks, identical experimental conditions were enforced throughout the study. In each cross-validation fold, the same held-out well served as the test sample across both models, while the remaining wells were used for training. This well-level K-fold scheme was implemented independently within each field (Danan and Azadegan North(AZNN)) and separately for each prediction target (NPHI, RHOB, and DT), yielding twelve fully independent models.

Furthermore, identical missingness masks were applied to the input logs of both frameworks, ensuring that each model faced the same depth intervals of synthetic data removal. Although numerical results varied across folds, the performance trends were consistent; therefore, representative outcomes for each target and field are reported. A consolidated overview of this unified evaluation configuration is now provided in Table 1 to improve clarity and reproducibility.

Statistical significance was assessed using the Wilcoxon signed-rank test applied to the well-level MAE values of the NPHI target. Nineteen paired samples (ten wells from Azadegan and nine from Danan) were used to compare the ConvLSTM model with the MICE+GBT workflow under identical cross-validation conditions. The Wilcoxon test was selected due to the non-normal distribution of MAE differences and the relatively small sample size. A significance level of 0.05 was used.

Table 1. Overal overview of evaluation configuration.

Field	Prediction target	Frameworks	# of Independent Models	Cross-Validation Scheme	Train Wells	Test Wells (per fold)	Missingness Enforcement
Danan	NPHI	MICE + GBT / ConvLSTM	2	Well-level K-fold (10 folds)	9 (rotating)	1 (rotating)	Identical masking for missing intervals applied across both models
	RHOB	MICE + GBT / ConvLSTM	2	Well-level K-fold (10 folds)	9 (rotating)	1 (rotating)	Identical masking for missing intervals applied across both models
	DT	MICE + GBT / ConvLSTM	2	Well-level K-fold (10 folds)	9 (rotating)	1 (rotating)	Identical masking for missing intervals applied across both models
Azadegan	NPHI	MICE + GBT / ConvLSTM	2	Well-level K-fold (10 folds)	9 (rotating)	1 (rotating)	Identical masking for missing intervals applied across both models
	RHOB	MICE + GBT / ConvLSTM	2	Well-level K-fold (10 folds)	9 (rotating)	1 (rotating)	Identical masking for missing intervals applied across both models
	DT	MICE + GBT / ConvLSTM	2	Well-level K-fold (10 folds)	9 (rotating)	1 (rotating)	Identical masking for missing intervals applied across both models

Uncertainty for ConvLSTM predictions was quantified using Monte Carlo dropout inference. During test-time evaluation, the dropout layers remained active, generating multiple stochastic forward passes for each depth sample. The predictive mean was computed from these samples, while the predictive standard deviation σ captured epistemic uncertainty. The resulting confidence interval (±2σ) represents an approximate 95% credible band of the ConvLSTM predictive distribution.

For the MICE+GBT workflow, uncertainty was derived from the dispersion of out-of-sample residuals under the same

well-level cross-validation splits used for model evaluation. The standard deviation of residuals across folds was taken as σ, providing a data-driven measure of variability. Although the two frameworks rely on different mechanisms, both uncertainty estimates reflect predictive variability under comparable train/test conditions and are consistently reported using the ±2σ notation.

3.8 Hyperparameter Selection Strategy

Both frameworks were trained under a unified tuning strategy to ensure comparability. Cross-validated searches were performed for ConvLSTM (filters, learning rate, dense width) and for GBT (n_estimators, learning rate, max_depth, subsampling ratio). Selection was based on minimizing validation MAE and MSE and ensuring stable convergence across folds.

3.9 Workflow Integration and Contributions

The methodologies integrate complementary strengths: MICE+GBT emphasizes interpretability and efficiency for feature-driven imputation, while ConvLSTM excels in capturing non-linear, sequential complexities without explicit feature engineering. Both were benchmarked via cross-validation and missingness tests, simulating Sarvak-specific challenges like borehole instability. Contributions include adaptable workflows for carbonate reservoirs, with empirical validation of method trade-offs (e.g., GBT's speed vs. ConvLSTM's accuracy in long gaps). Results will inform practical applications, enhancing subsurface characterization reliability.

4 Results and Discussions

4.1 Overall Performance Trends

Both the statistical-ensemble framework (MICE+GBT) and the deep learning framework (ConvLSTM) successfully reconstructed missing well logs in the Sarvak Formation; however, their efficacy varied according to the target petrophysical property and prevailing reservoir conditions. Quantitative assessments, employing metrics such as R, R^2, MSE, and MAE, revealed that the GBT model consistently outperformed ConvLSTM across the majority of evaluated scenarios (Table 1). For NPHI, the GBT model attained R value equals to 0.92 and R^2 of 0.84, with a mean error of 0.011, whereas ConvLSTM exhibited marginally lower performance with R = 0.91, R^2 = 0.71, and MAE = 0.015. Reconstructions of RHOB similarly favored GBT with R^2 = 0.67 vs. 0.45; and MAE = 0.037 vs. 0.047. The most pronounced disparity emerged in DT, where GBT delivered stable predictions with R = 0.90, R^2 = 0.75, and MAE ≈ 2.18 μs/ft, in contrast to ConvLSTM, which exhibited difficulties in convergence and produced substantially elevated errors (MAE > 58 μs/ft). This divergence highlights the superior robustness of ensemble-based methods when applied to complex carbonate datasets.

To further investigate the differences in ConvLSTM performance across prediction targets, training-diagnostic curves were analyzed for all models. Figures 3-8 illustrate the validation-loss evolution for NPHI, RHOB, and DT in both the Danan and Azadegan fields. RHOB demonstrated smooth and monotonic convergence in all cases, reflecting the relative stability of density measurements. NPHI showed mild oscillatory behavior, particularly in the Azadegan field, consistent with the sensitivity of neutron-porosity to spectral-gamma noise and abrupt facies variability.

In contrast, the DT target exhibited markedly different convergence dynamics. Both fields showed extremely high initial loss values, followed by partial convergence and, in some cases, mild divergence. This behavior reflects the intrinsic complexity of acoustic travel-time signals in heterogeneous carbonate reservoirs rather than a failure of the optimization process. The ConvLSTM model captured local sequential trends but remained sensitive to field-specific borehole conditions and high-frequency noise, contributing to the higher error magnitudes reported for DT. These diagnostics highlight that the underperformance of ConvLSTM for DT is fundamentally data-driven, reinforcing the robustness of the ensemble-based GBT approach for sonic-log reconstruction in carbonate settings.

A concise description of the key architectural configurations and hyperparameters has been incorporated into the Methodology section. By grounding both frameworks in their published baseline architectures (Mukherjee, et al., 2024; Hallam, et al., 2022) and by reporting all relevant training settings, the study ensures that the full workflow can be reproduced using publicly available implementations.

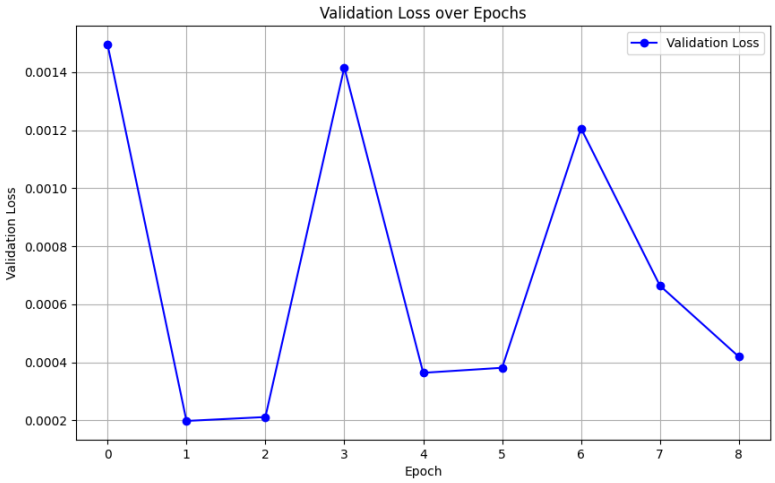

Figure 3. Loss behaviour plot for NPHI prediction in Azadegan oilfield.

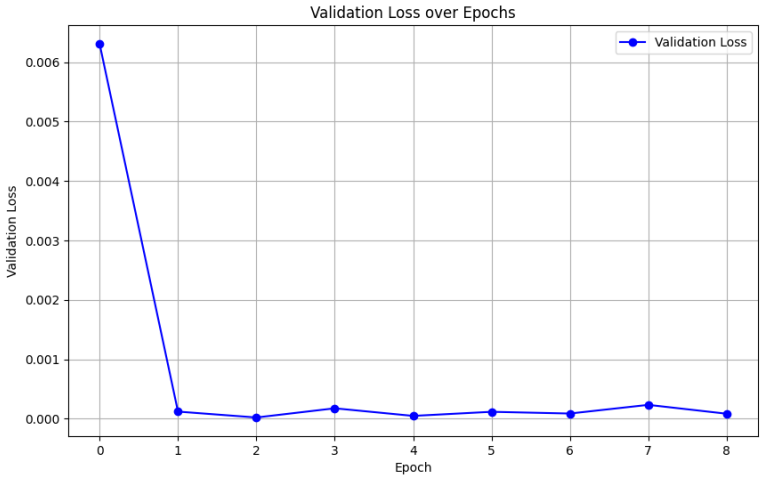

Figure 4. Loss behaviour plot for RHOB prediction in Azadegan oilfield.

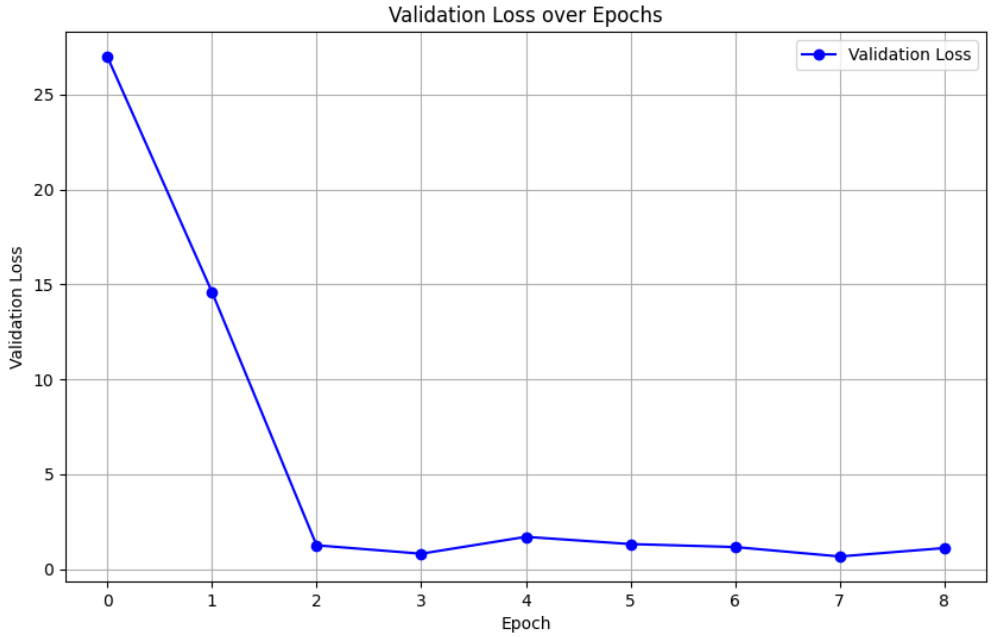

Figure 5. Loss behaviour plot for DT prediction in Azadegan oilfield.

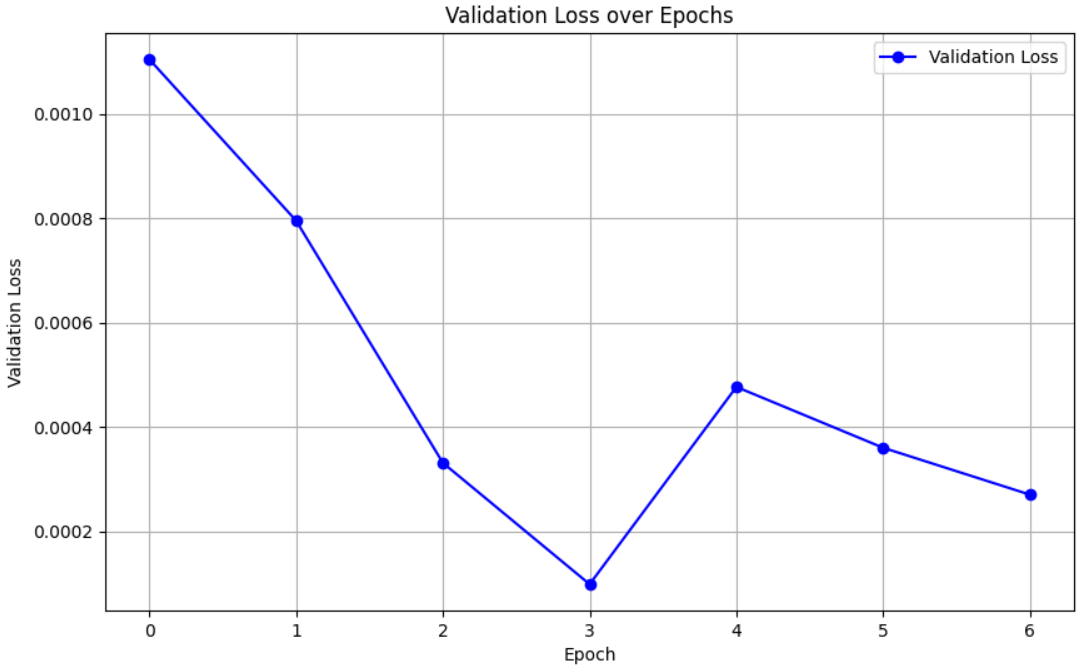

Figure 6. Loss behaviour plot for NPHI prediction in Danan oilfield.

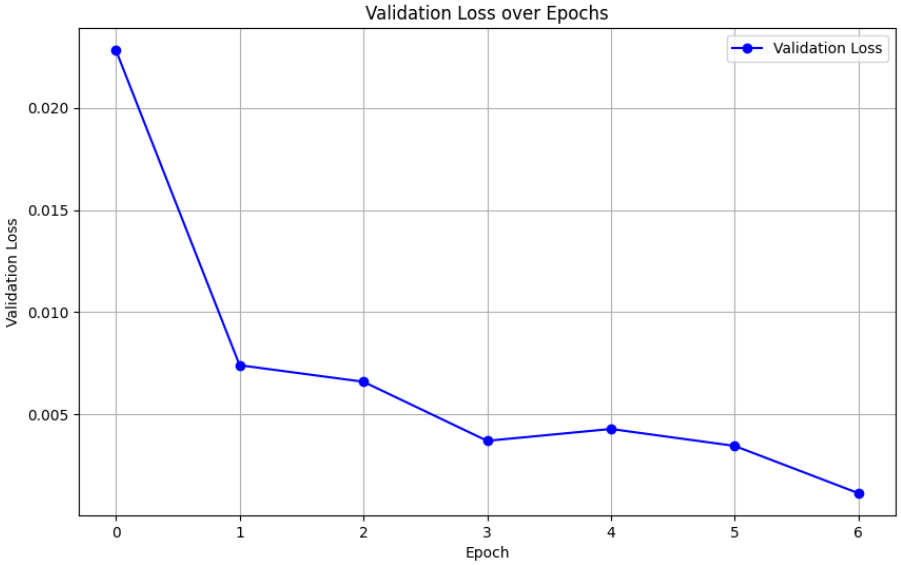

Figure 7. Loss behaviour plot for RHOB prediction in Danan oilfield.

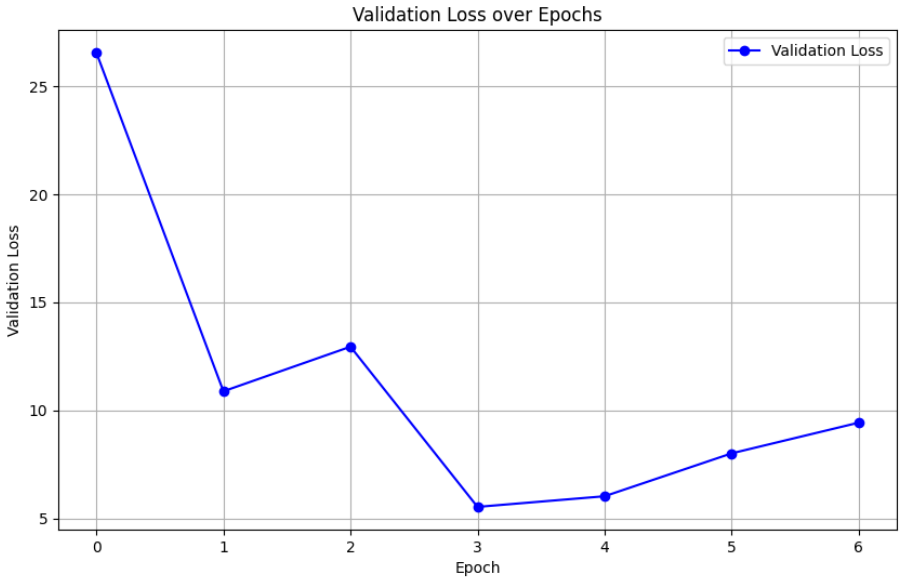

Figure 8. Loss behaviour plot for DT prediction in Danan oilfield.

The Wilcoxon signed-rank test performed on the NPHI MAE values confirmed that the performance gain of MICE+GBT over ConvLSTM is statistically significant. The MAE differences were consistently positive across all wells, resulting in a p-value < 0.001. This indicates that the superiority of GBT is not attributable to random variation but represents a systematic improvement. Since RHOB and DT exhibited even larger performance gaps (Table 2), these significance results are expected to generalize across all target logs.

4.2 Depth-Wise Predictions and

Uncertainty

Depth-aligned comparisons of predicted and observed logs for representative wells in the Danan and Azadegan fields are illustrated in Figures 9-14. The GBT-predicted profiles closely mirrored the observed data, even in intervals characterized by high lithological heterogeneity. In comparison, ConvLSTM predictions (Figures 15-20) aligned reasonably well in smoother intervals but deviated markedly in zones featuring abrupt facies transitions or borehole instability. Shaded confidence intervals (±2σ) indicate that the majority of true measurements resided within the modeled uncertainty bands, particularly for GBT, whereas ConvLSTM intervals expanded considerably in heterogeneous layers.

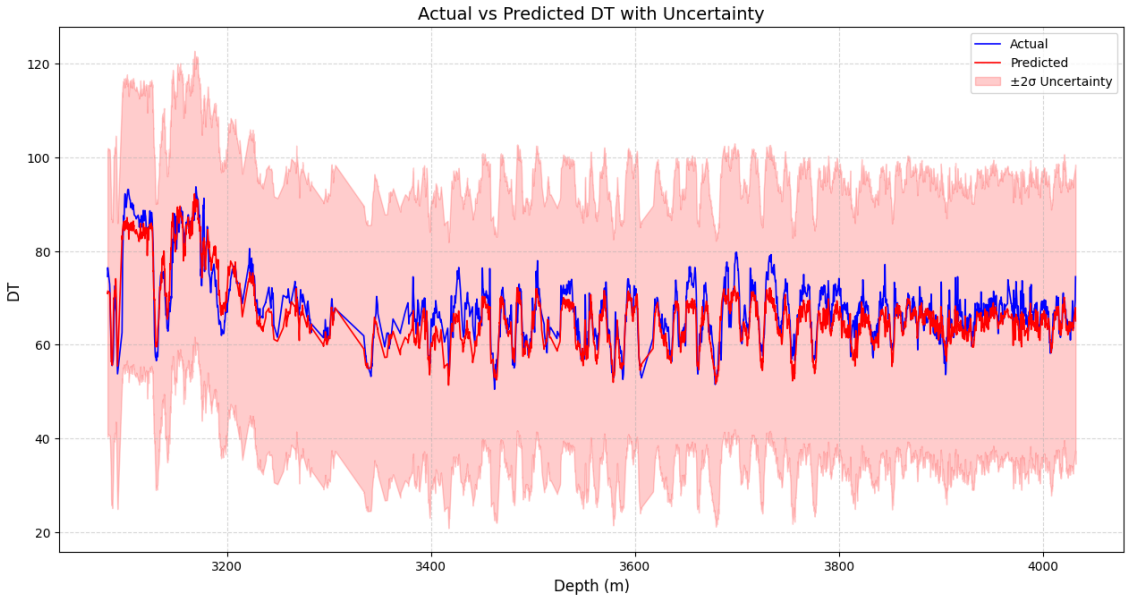

Figure 9. Actual vs. predicted DT with uncertainty for AZNN wells by GBT.

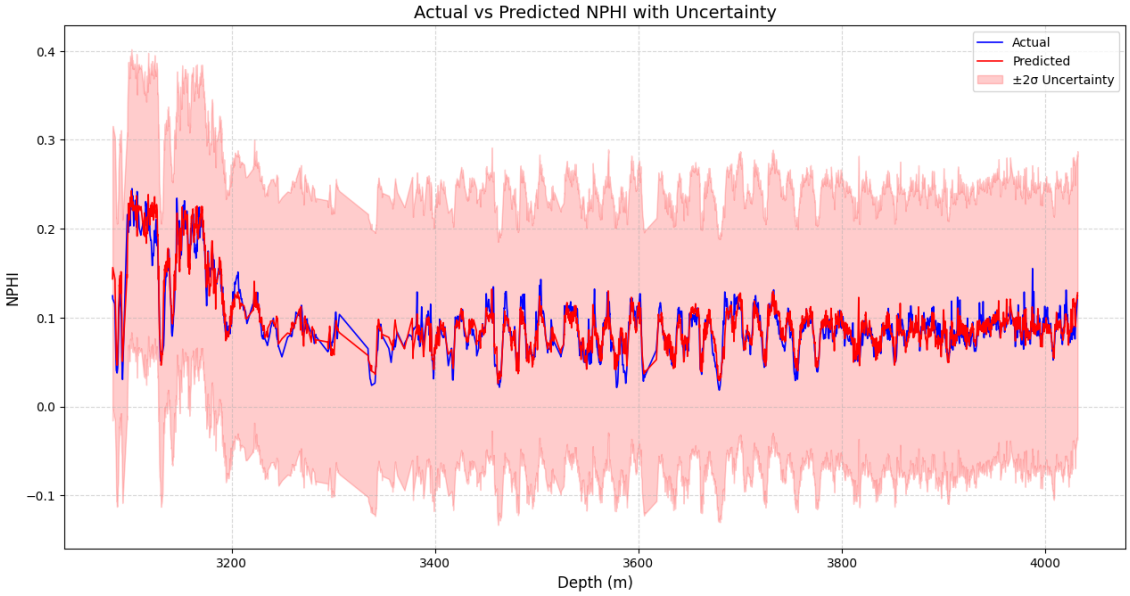

Figure 10. Actual vs. predicted NPHI with uncertainty for AZNN wells by GBT.

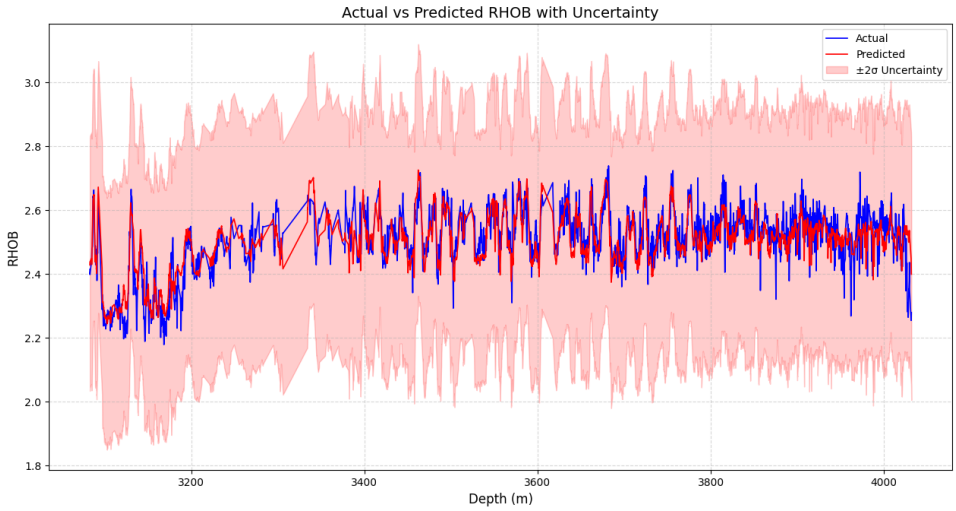

Figure 11. Actual vs. predicted RHOB with uncertainty for AZNN wells by GBT.

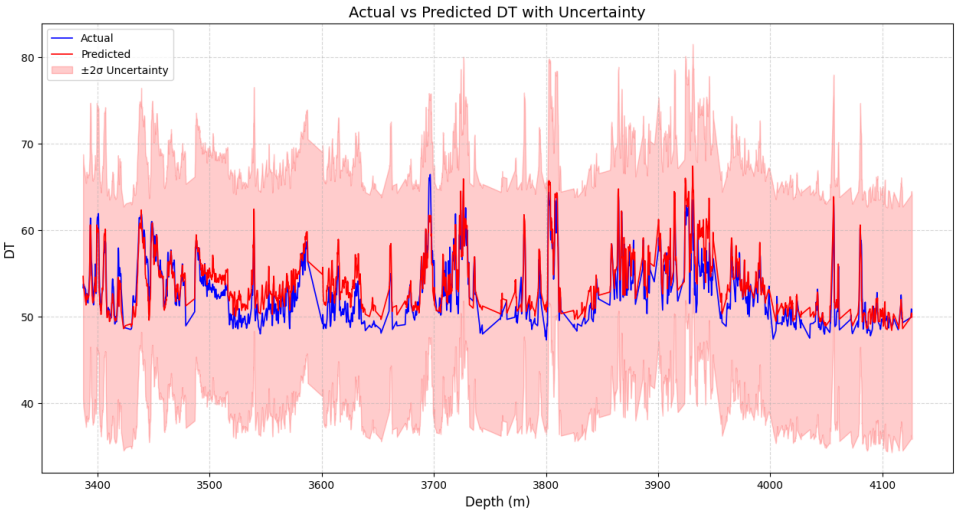

Figure 12. Actual vs. predicted DT with uncertainty for DA wells by GBT.

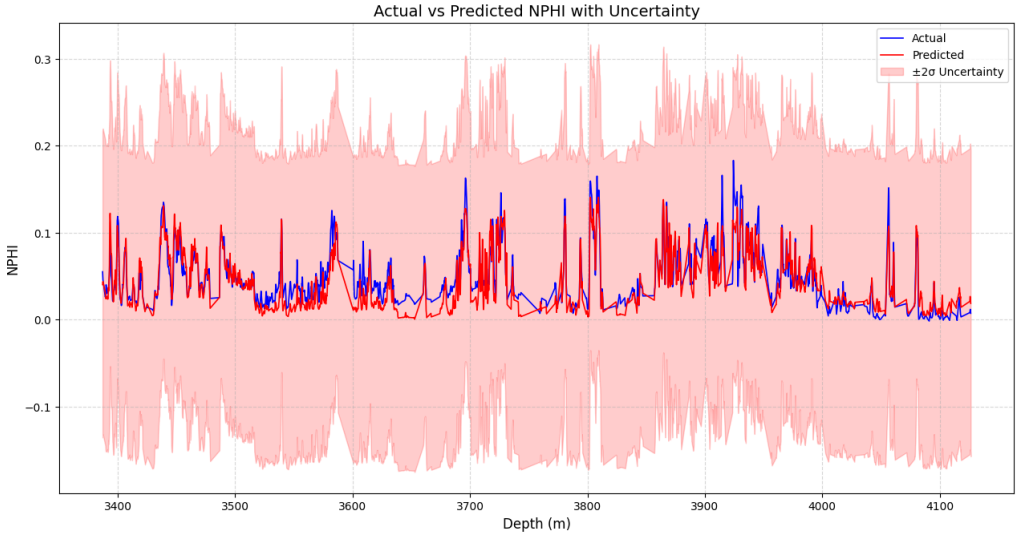

Figure 13. Actual vs. predicted NPHI with uncertainty for DA wells by GBT.

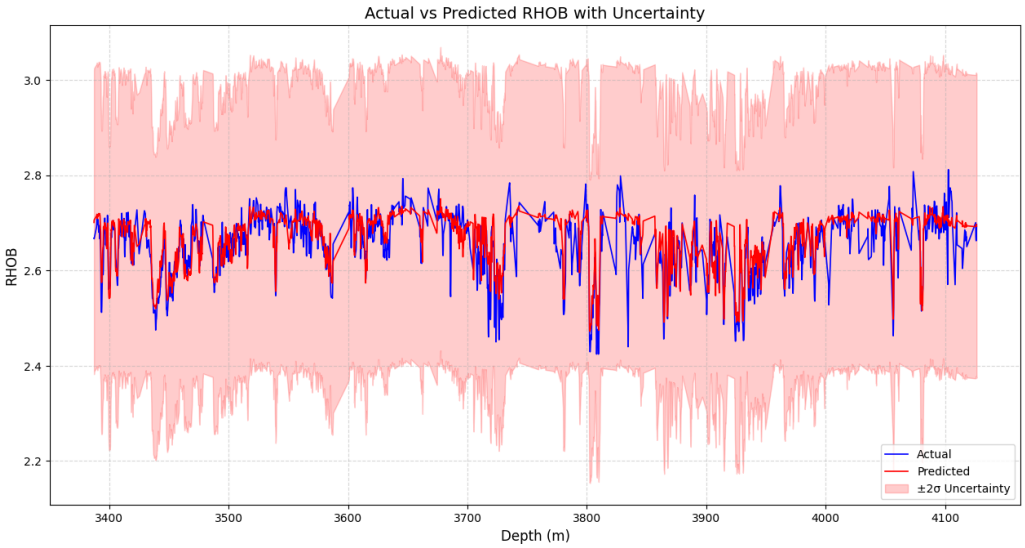

Figure 14. Actual vs. predicted RHOB with uncertainty for DA wells by GBT.

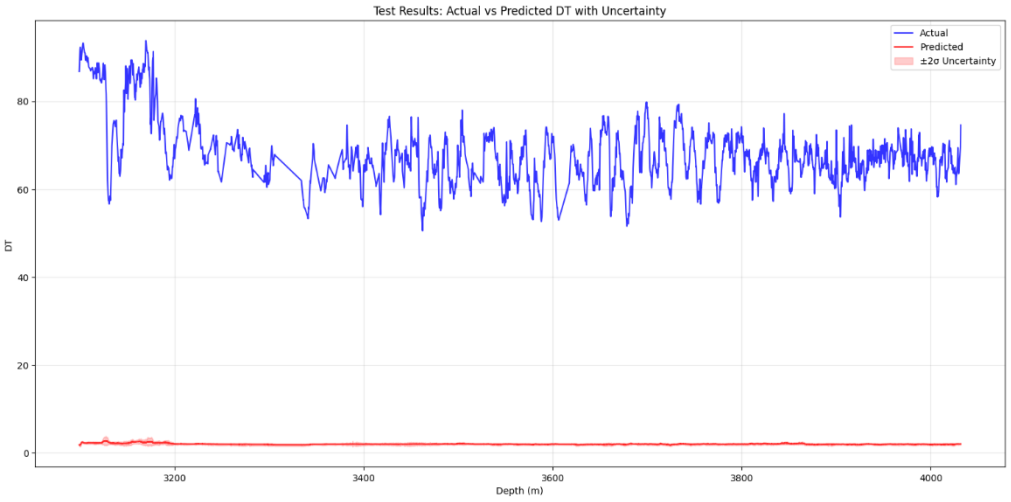

Figure 15. Actual vs. predicted DT with uncertainity for AZNN wells by ConvLSTM.

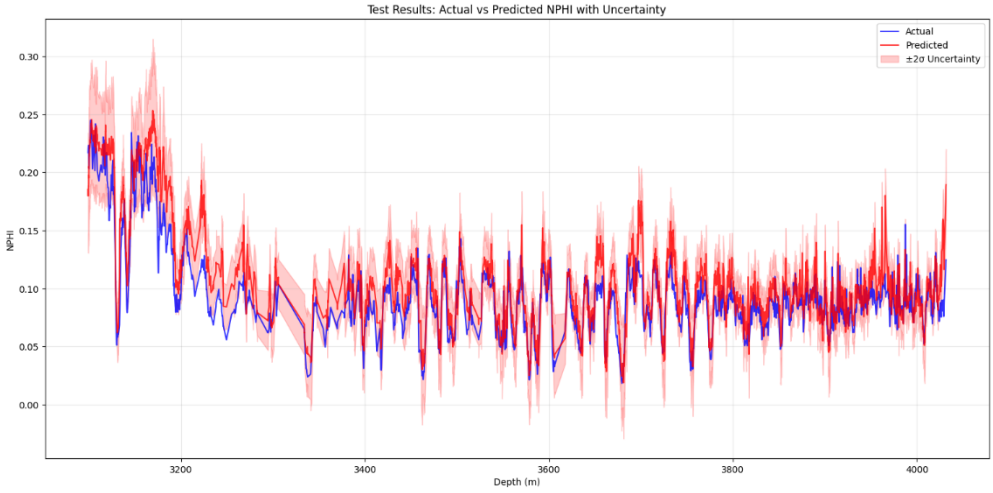

Figure 16. Actual vs. predicted NPHI with uncertainity for AZNN wells by ConvLSTM.

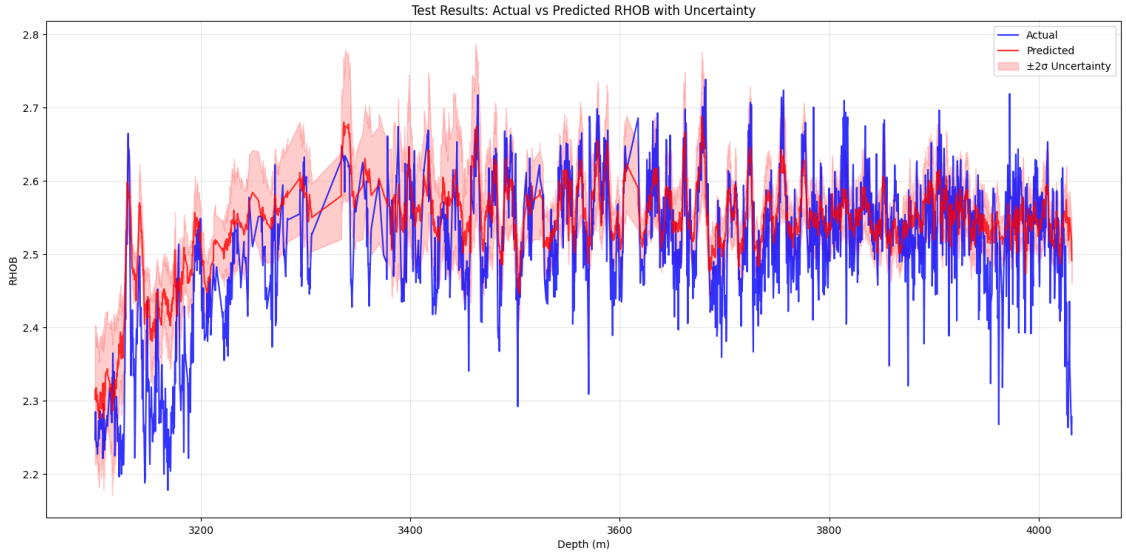

Figure 17. Actual vs. predicted RHOB with uncertainity for AZNN wells by ConvLSTM.

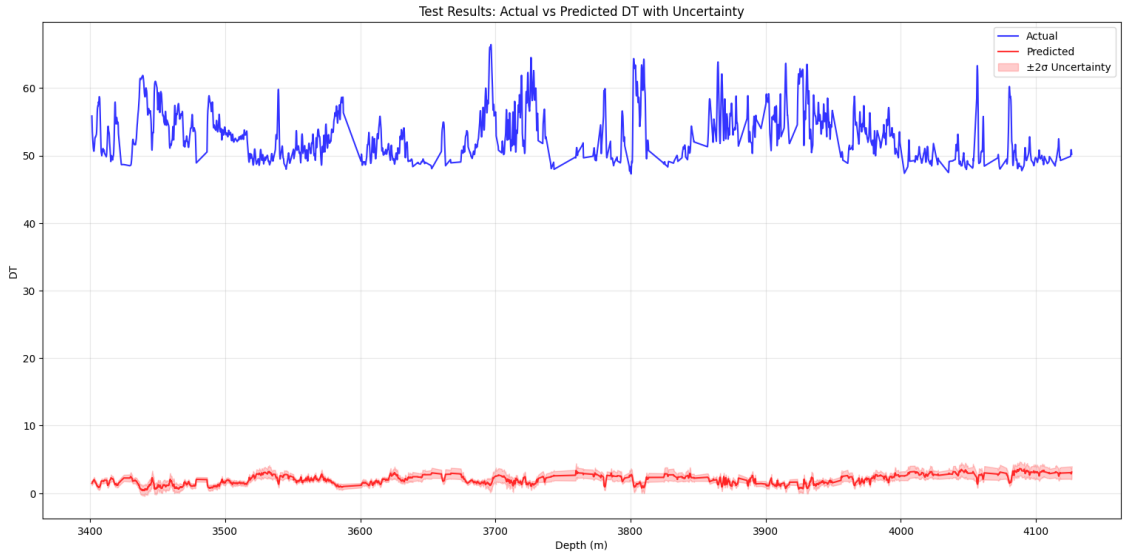

Figure 18. Actual vs. predicted DT with uncertainity for DA wells by ConvLSTM.

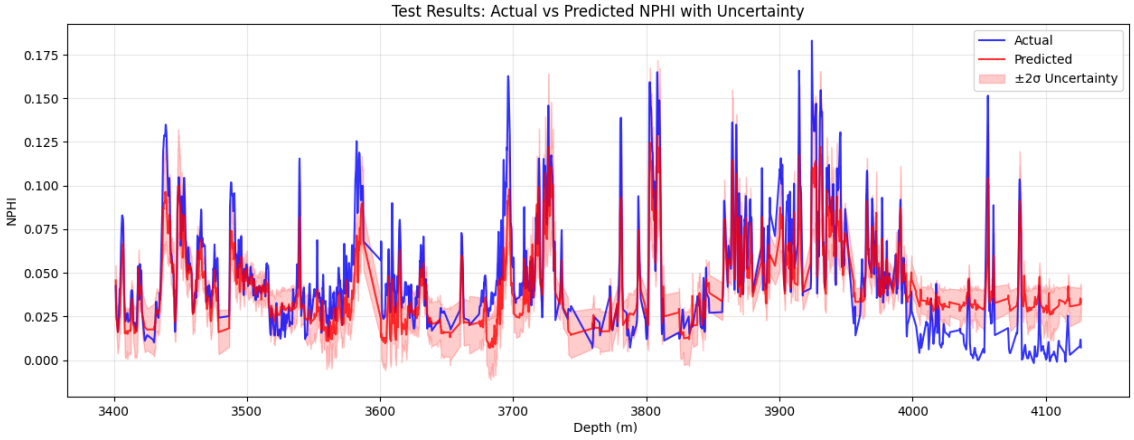

Figure 19. Actual vs. predicted NPHI with uncertainity for DA wells by ConvLSTM.

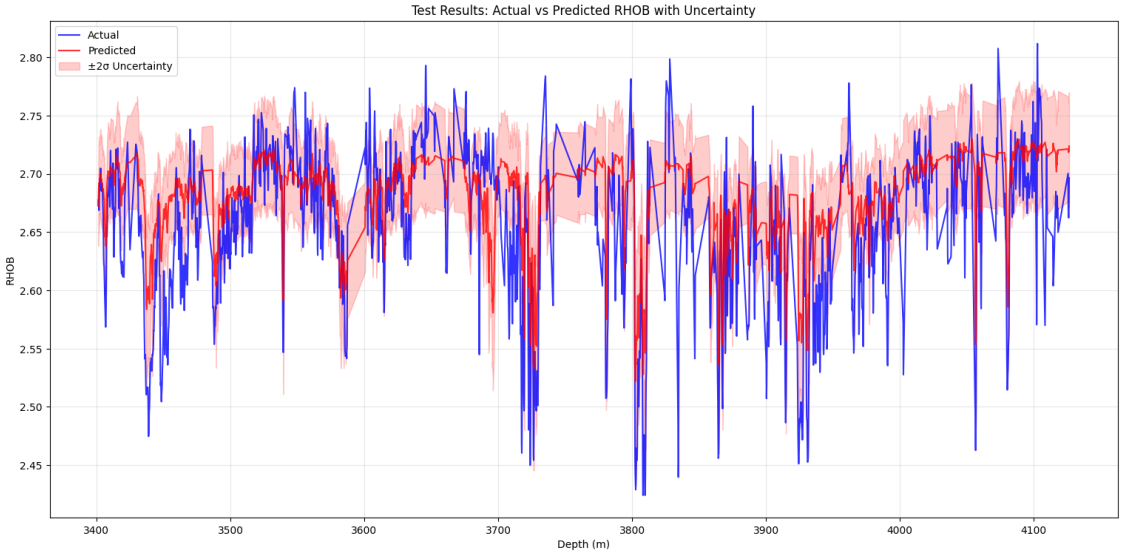

Figure 20. Actual vs. predicted RHOB with uncertainity for DA wells by ConvLSTM.

4.3 Scatter Plots and Correlation

Scatter plots comparing actual versus predicted values (Figures 21-26) corroborate these observations. For GBT, data points clustered tightly along the 1:1 reference line, exhibiting minimal dispersion and strong statistical alignment. Conversely, ConvLSTM scatter plots (Figures 27-32) displayed broader spreads, with systematic underestimation of high-end values for NPHI and DT, indicative of heightened sensitivity to extreme ranges and diminished generalization capabilities.

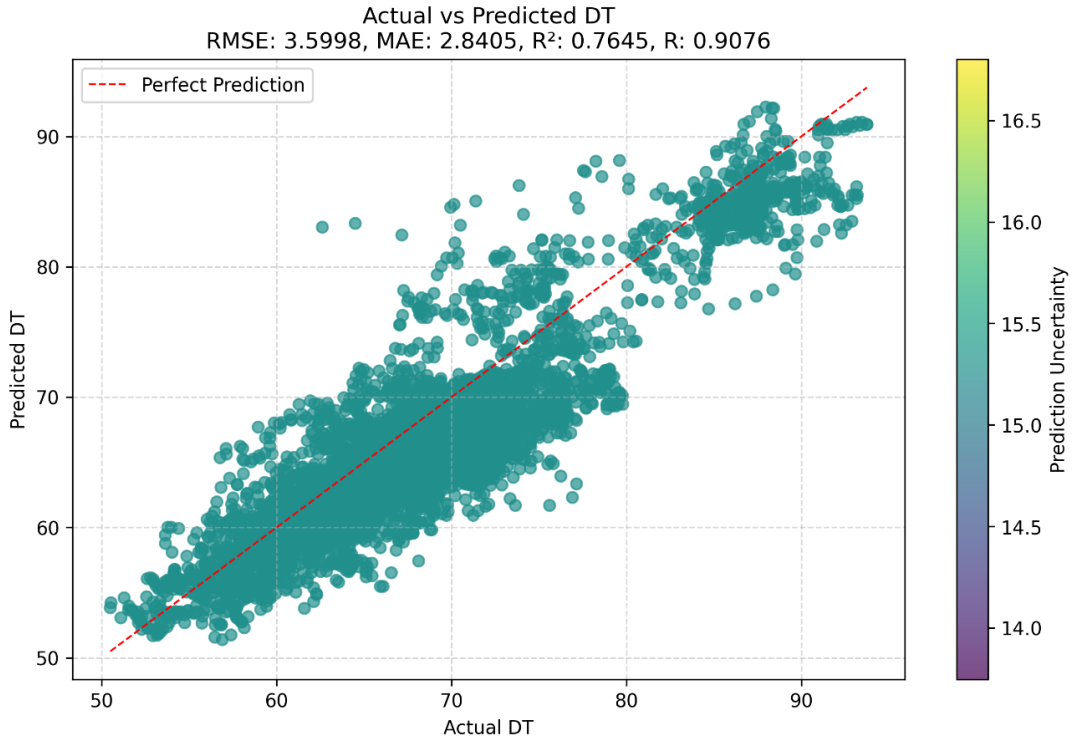

Figure 21. Scatter plot comparing actual versus predicted DT values for AZNN wells by GBT.

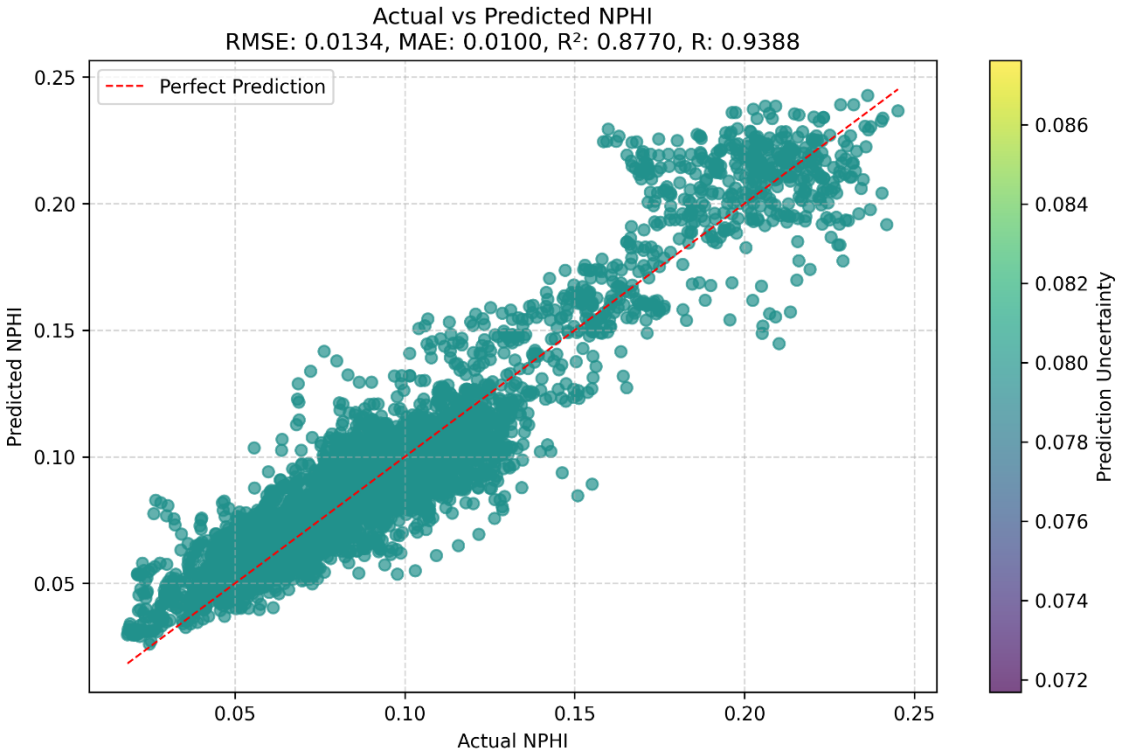

Figure 22. Scatter plot comparing actual versus predicted NPHI values values for AZNN wells by GBT.

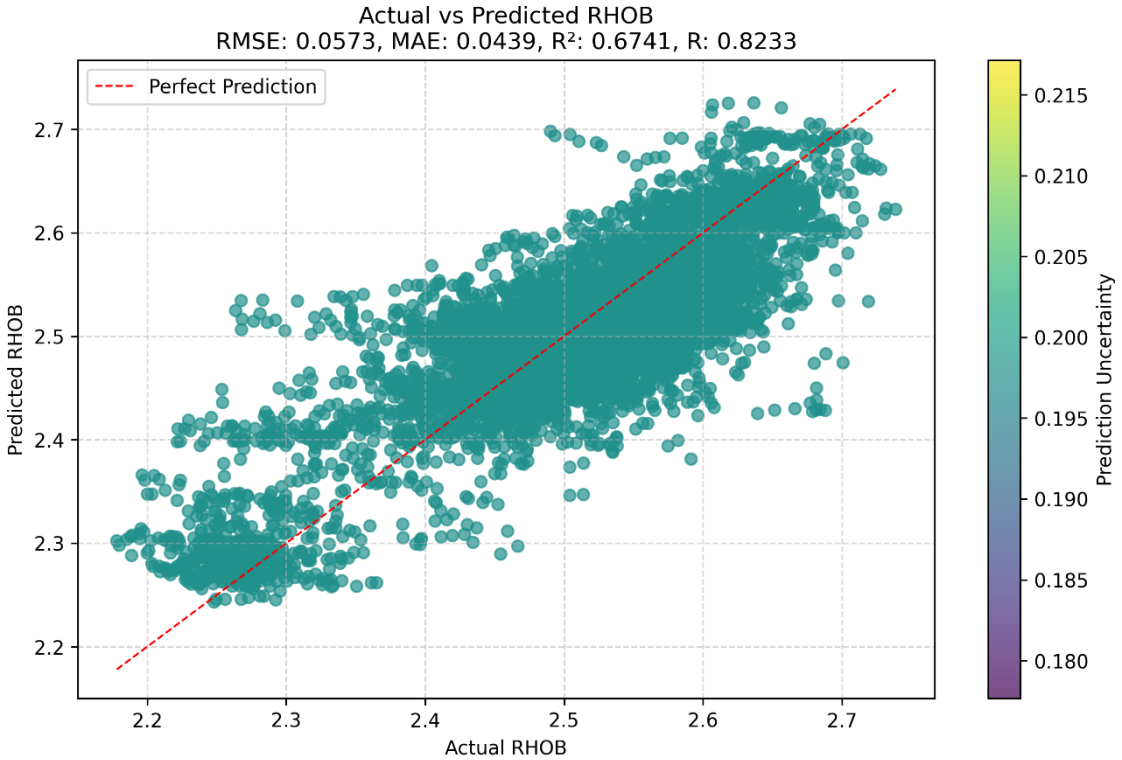

Figure 23. Scatter plot comparing actual versus predicted RHOB values values for AZNN wells by GBT.

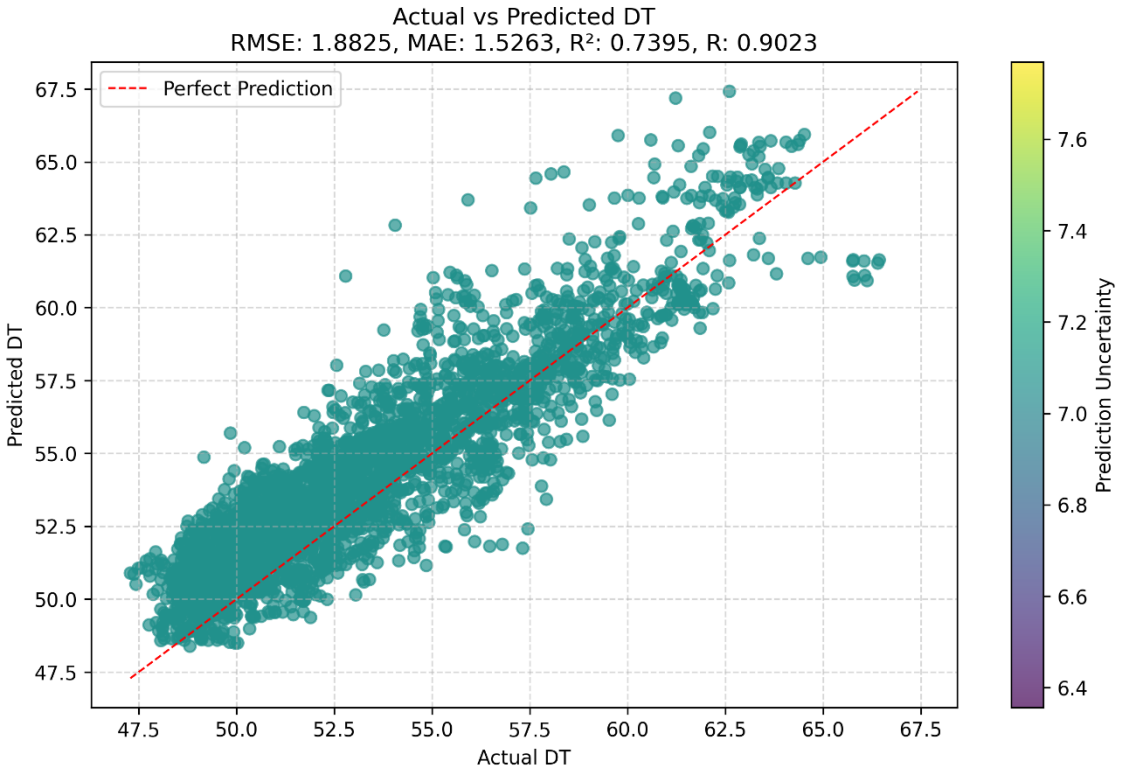

Figure 24. Scatter plot comparing actual versus predicted DT values values for DA wells by GBT.

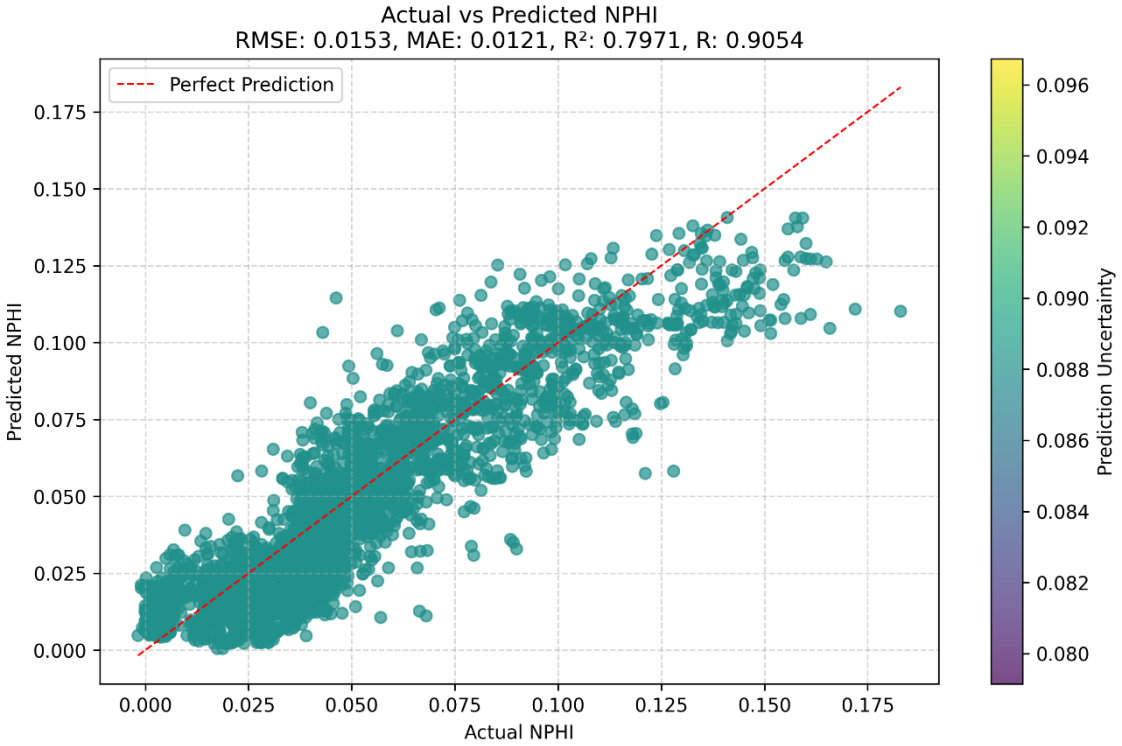

Figure 25. Scatter plot comparing actual versus predicted NPHI values values for DA wells by GBT.

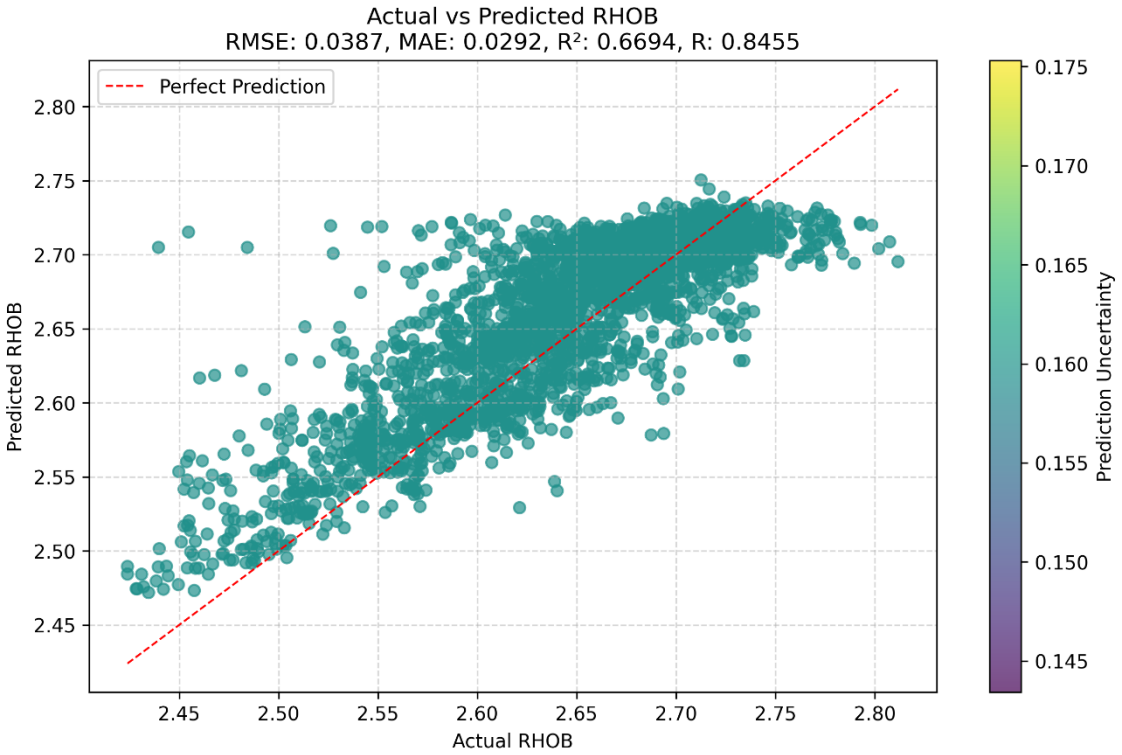

Figure 26. Scatter plot comparing actual versus predicted RHOB values values for DA wells by GBT.

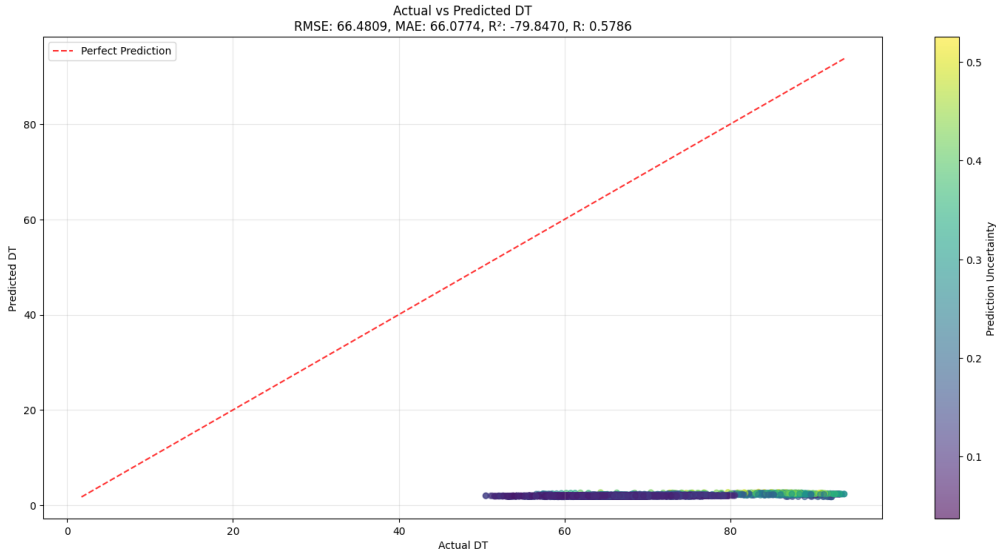

Figure 27. Scatter plot comparing actual versus predicted DT values for AZNN wells by ConvLSTM.

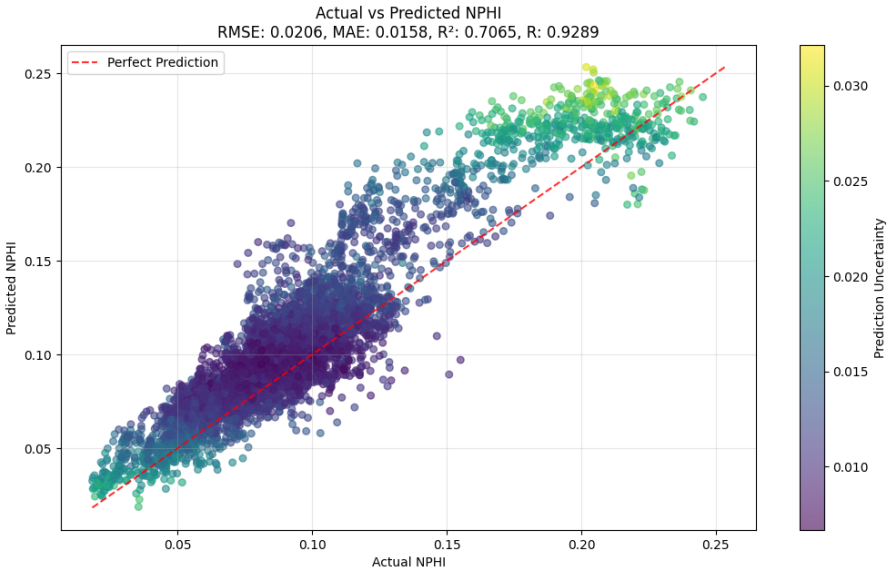

Figure 28. Scatter plot comparing actual versus predicted NPHI values for AZNN wells by ConvLSTM.

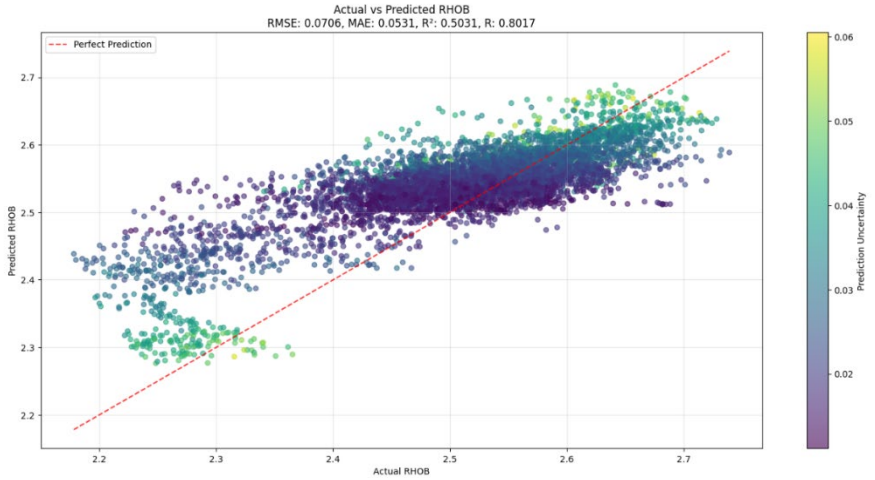

Figure 29. Scatter plot comparing actual versus predicted RHOB values for AZNN wells by ConvLSTM.

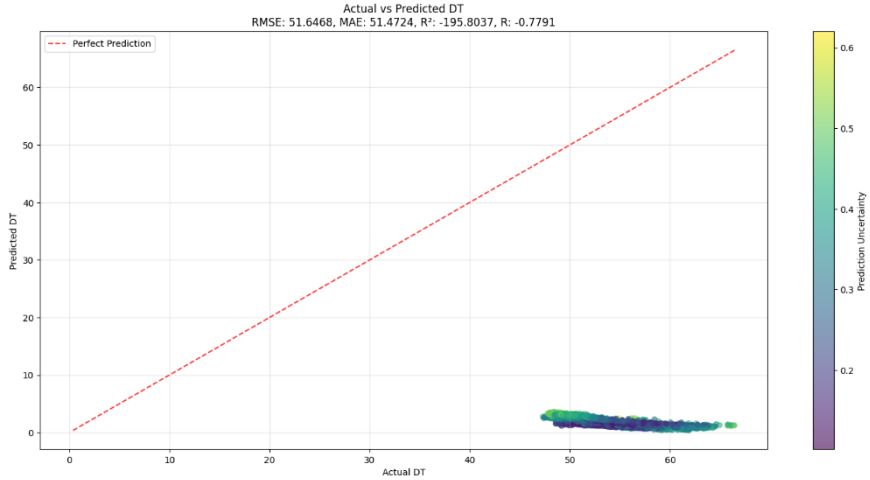

Figure 30. Scatter plot comparing actual versus predicted DT values for DA wells by ConvLSTM.

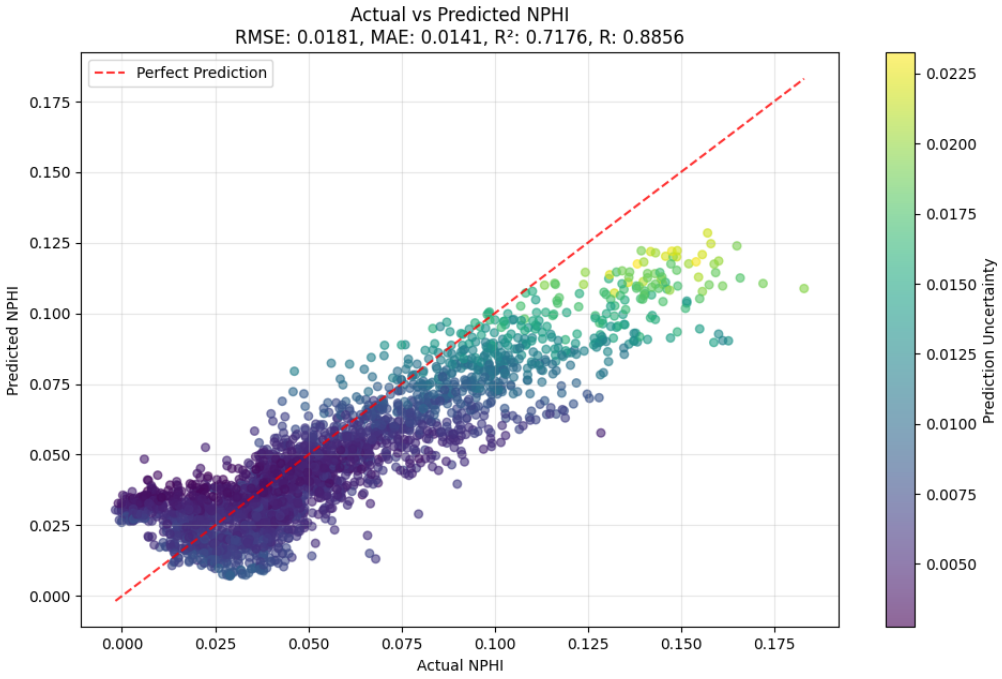

Figure 31. Scatter plot comparing actual versus predicted NPHI values for DA wells by ConvLSTM.

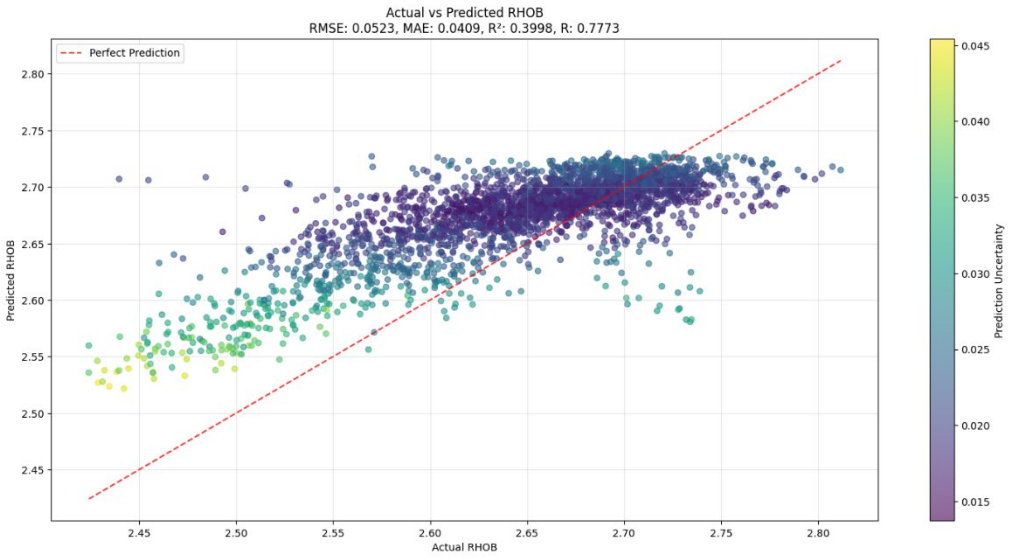

Figure 32. Scatter plot comparing actual versus predicted RHOB values for DA wells by ConvLSTM.

4.4 Error Distributions

Histograms and boxplots of prediction residuals (Figures 33-38) provide further evidence of methodological robustness. Residuals from GBT were symmetrically distributed around zero, with narrow interquartile ranges, signifying consistent predictive stability. In contrast, ConvLSTM residuals (Figures 39-44) demonstrated wider spreads and numerous extreme outliers, especially for RHOB and DT. The heavy-tailed nature of ConvLSTM's error distributions underscores its instability in the presence of carbonate heterogeneity and noise.

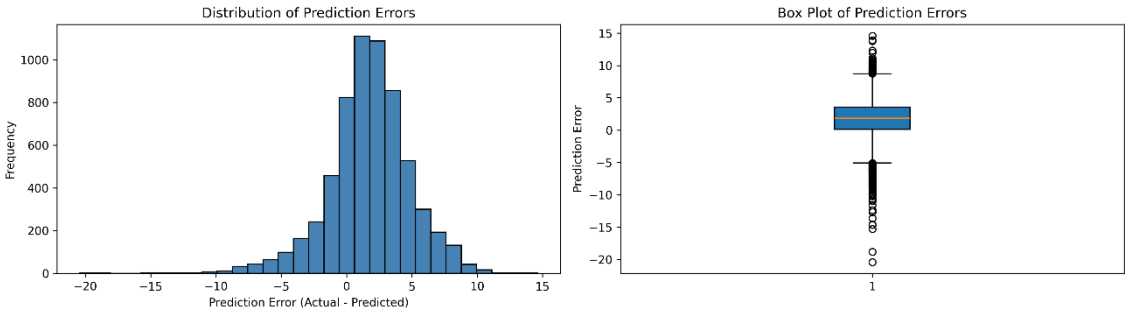

Figure 33. Histogram and boxplot of prediction residuals of DT for AZNN wells by GBT.

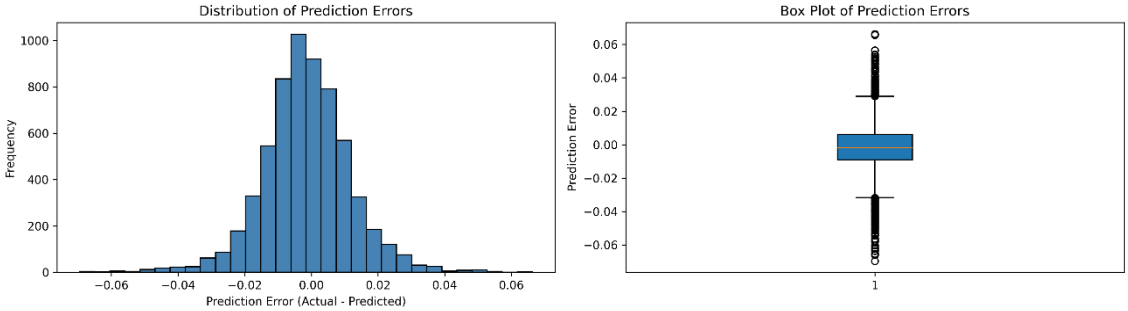

Figure 34. Histogram and boxplot of prediction residuals of NPHI for AZNN wells by GBT.

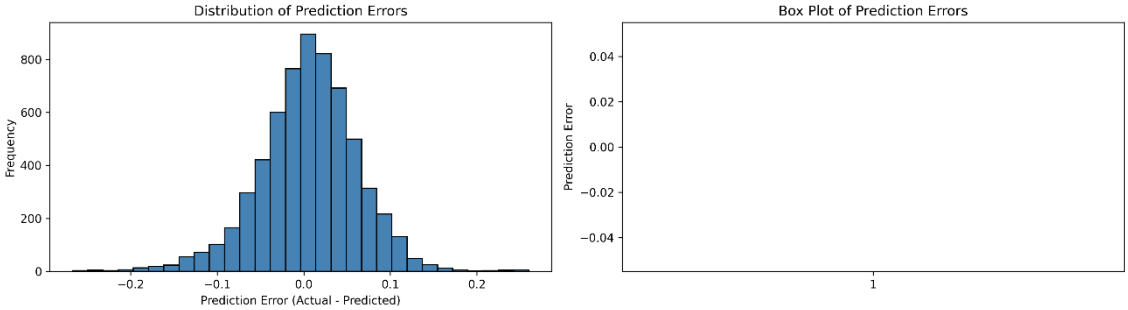

Figure 35. Histogram and boxplot of prediction residuals of RHOB for AZNN wells by GBT.

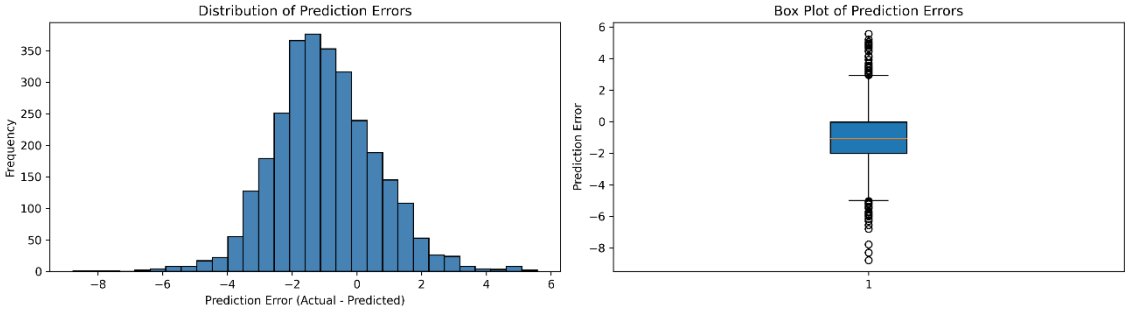

Figure 36. Histogram and boxplot of prediction residuals of DT for DA wells by GBT.

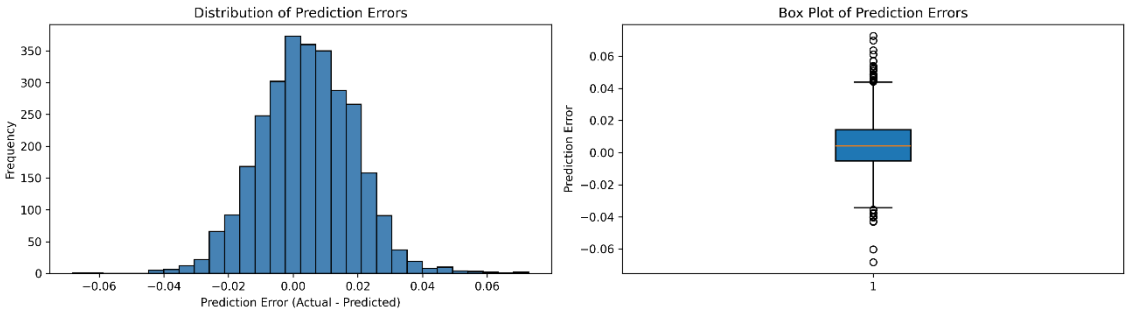

Figure 37. Histogram and boxplot of prediction residuals of NPHI for DA wells by GBT.

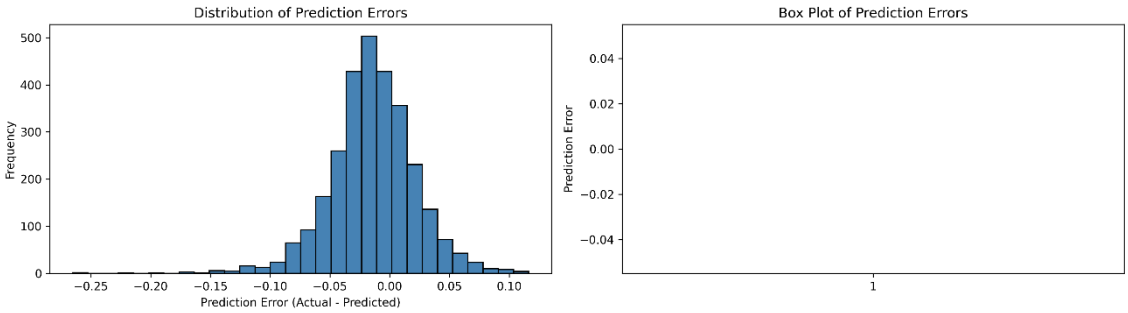

Figure 38. Histogram and boxplot of prediction residuals of RHOB for DA wells by GBT.

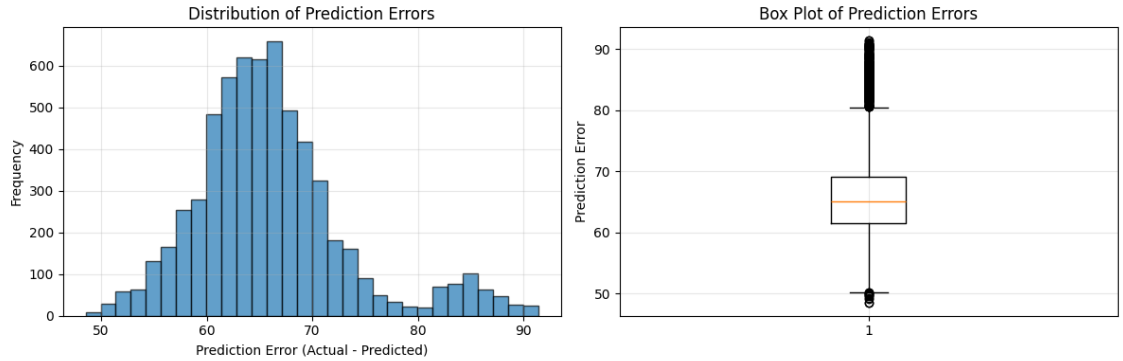

Figure 39. Histogram and boxplot of prediction residuals of DT for AZNN wells by ConvLSTM.

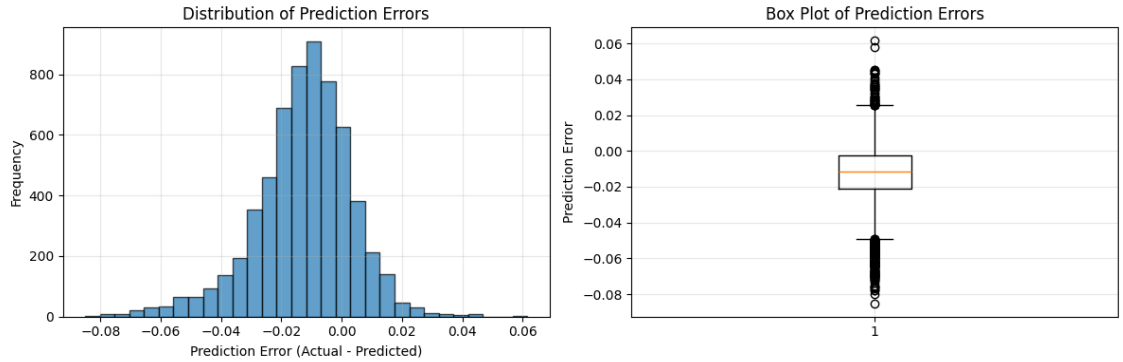

Figure 40. Histogram and boxplot of prediction residuals of NPHI for AZNN wells by ConvLSTM.

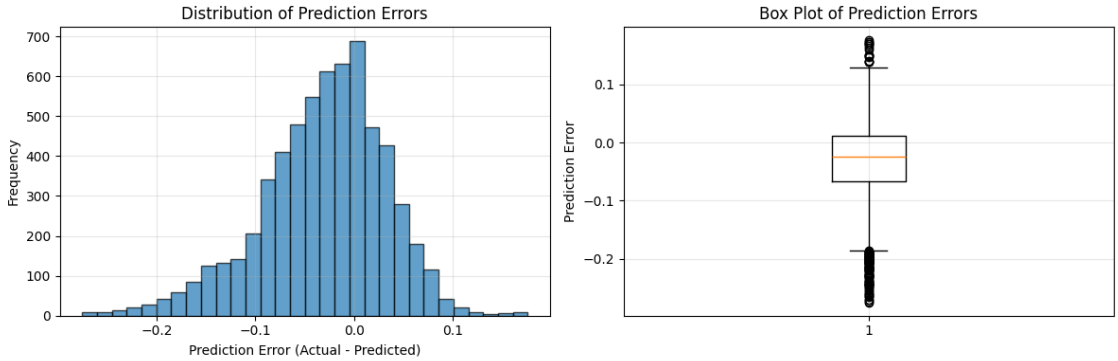

Figure 41. Histogram and boxplot of prediction residuals of RHOB for AZNN wells by ConvLSTM.

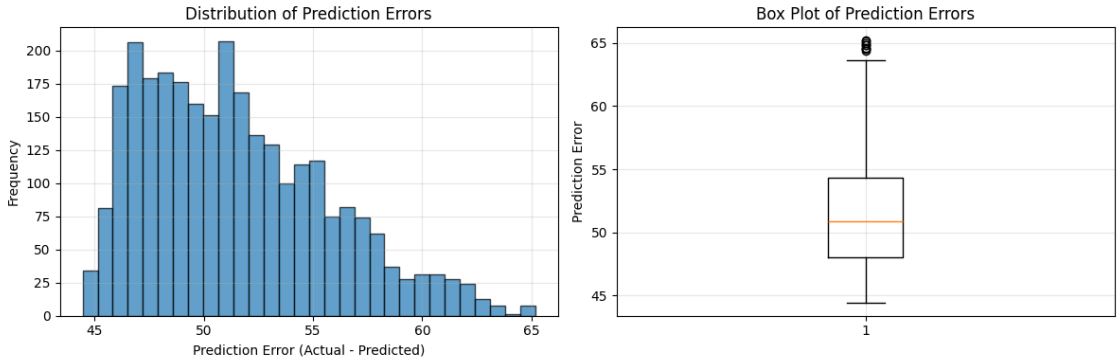

Figure 42. Histogram and boxplot of prediction residuals of DT for DA wells by ConvLSTM.

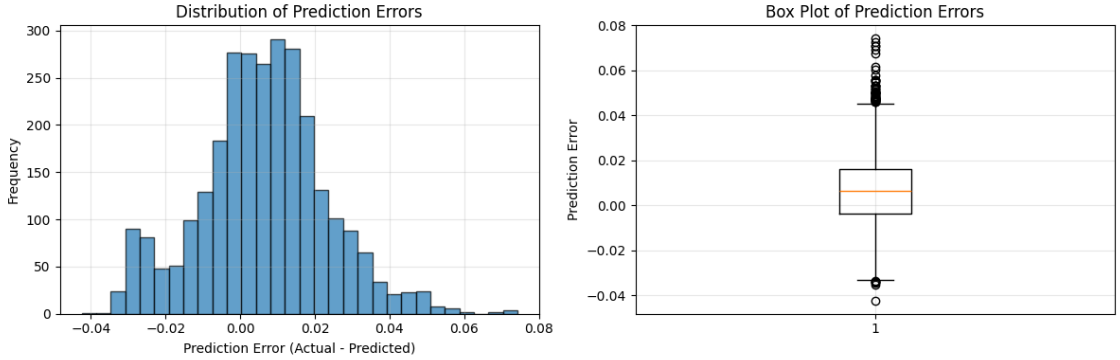

Figure 43. Histogram and boxplot of prediction residuals of NPHI for DA wells by ConvLSTM.

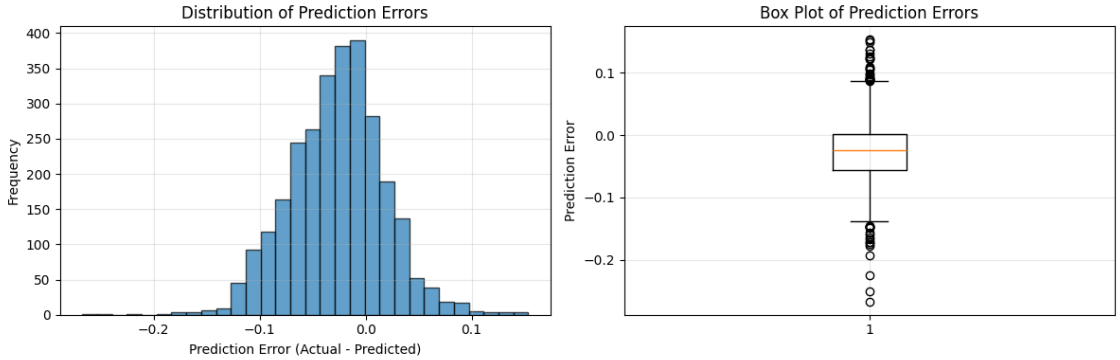

Figure 44. Histogram and boxplot of prediction residuals of RHOB for DA wells by ConvLSTM.

4.5 Well-Specific Comparisons

Performance disparities were particularly evident in well-by-well analyses. In test wells from the Danan field (Figures 45-56), GBT achieved reductions in MAE and MSE of up to 40% relative to ConvLSTM. In the Azadegan field (Figures 57-68), marked by greater heterogeneity, GBT sustained robust performance for NPHI and RHOB, whereas ConvLSTM experienced notable degradation. For DT, GBT maintained stability across both fields, while ConvLSTM exhibited significant divergence. These bar-chart comparisons affirm the enhanced generalization of ensemble models across diverse carbonate environments.

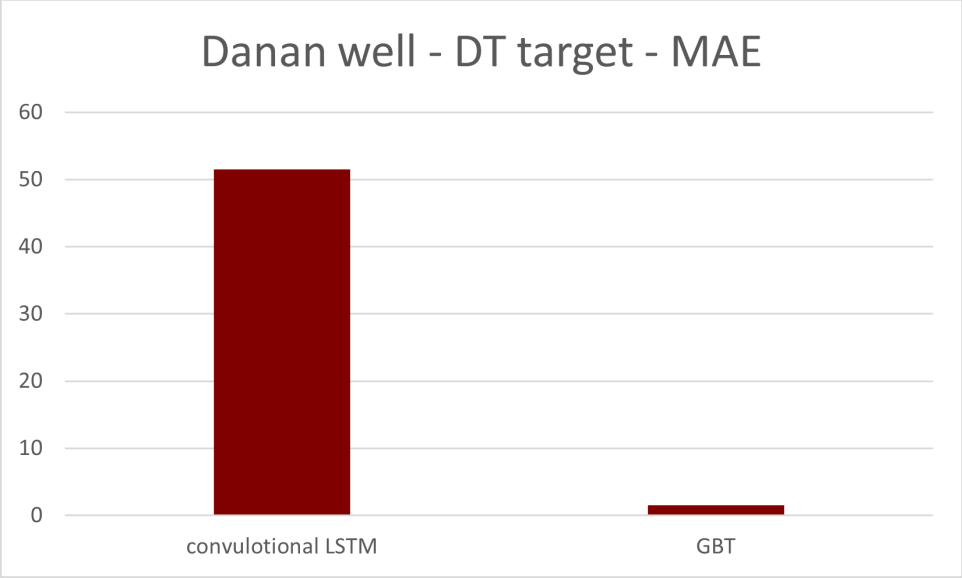

Figure 45. Well-Specific Comparison of ConvLSTM and GBT, DT target MAE for Danan oil field.

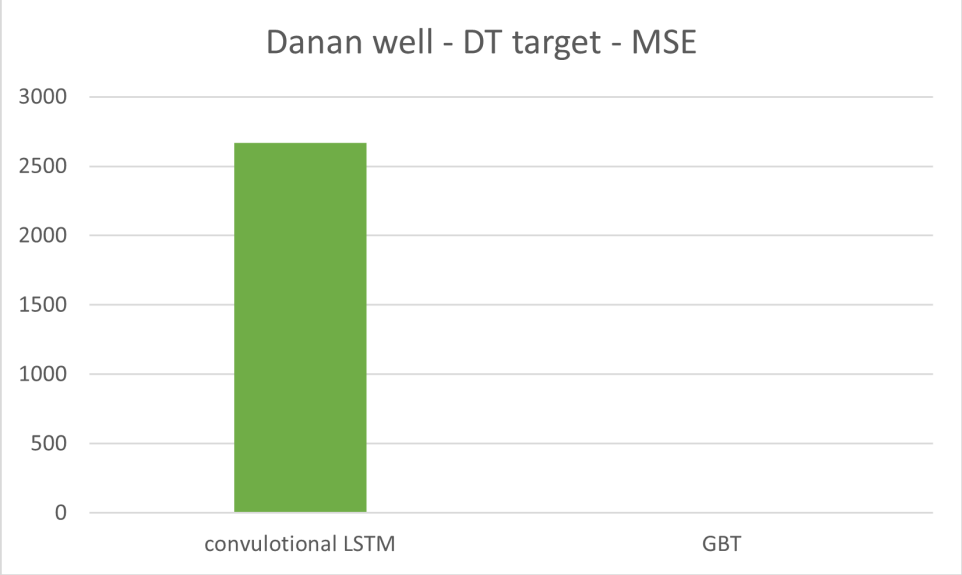

Figure 46. Well-Specific Comparison of ConvLSTM and GBT, DT target MSE for Danan oil field.

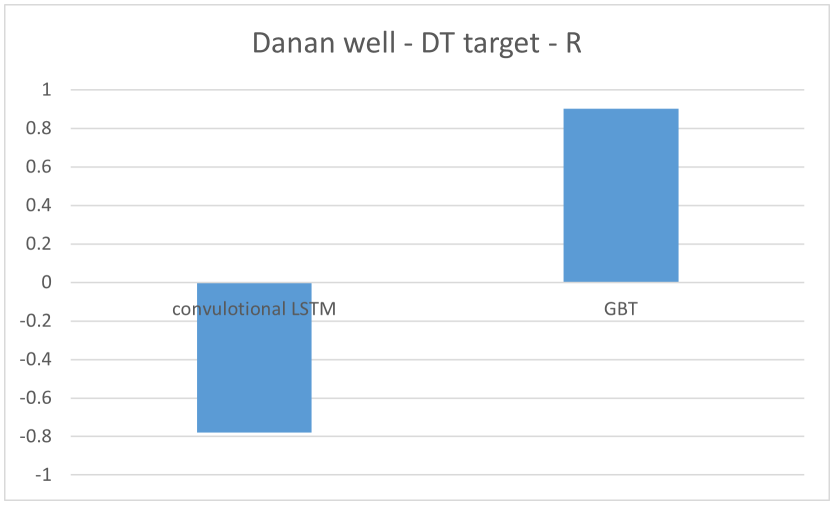

Figure 47. Well-Specific Comparison of ConvLSTM and GBT, DT target R for Danan oil field.

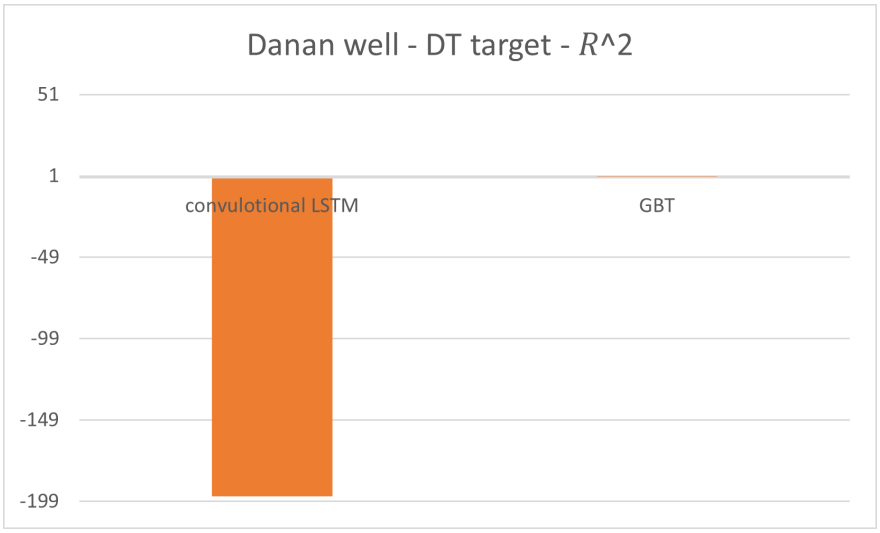

Figure 48. Well-Specific Comparison of ConvLSTM and GBT, DT target R^2 for Danan oil field.

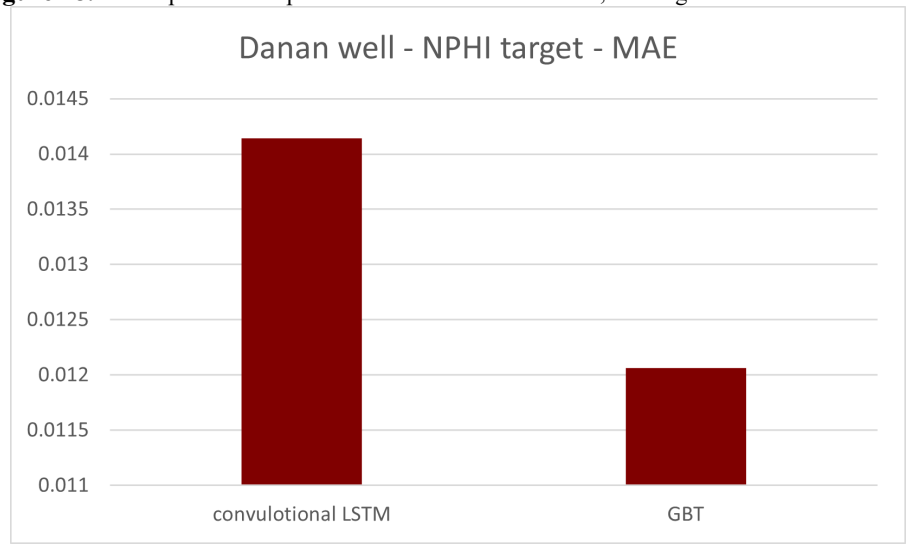

Figure 49. Well-Specific Comparison of ConvLSTM and GBT, NPHI target MAE for Danan oil field.

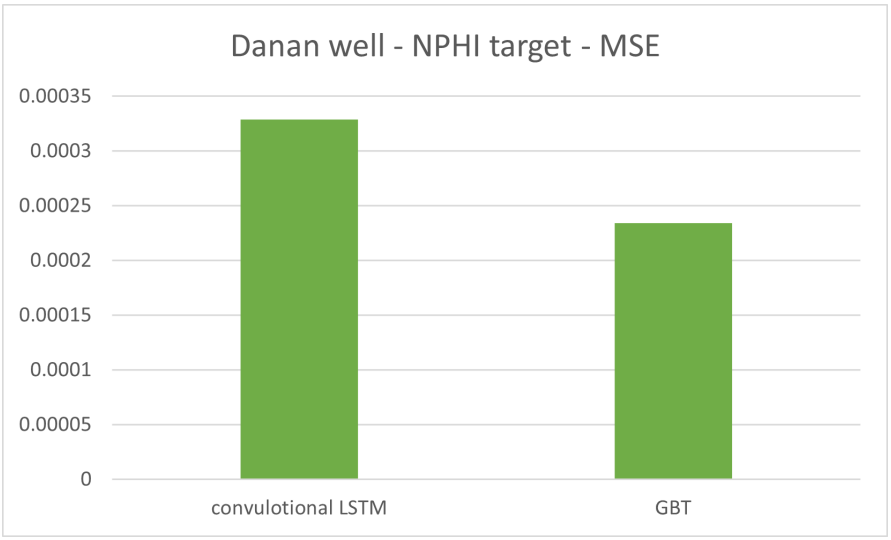

Figure 50. Well-Specific Comparison of ConvLSTM and GBT, NPHI target MSE for Danan oil field.

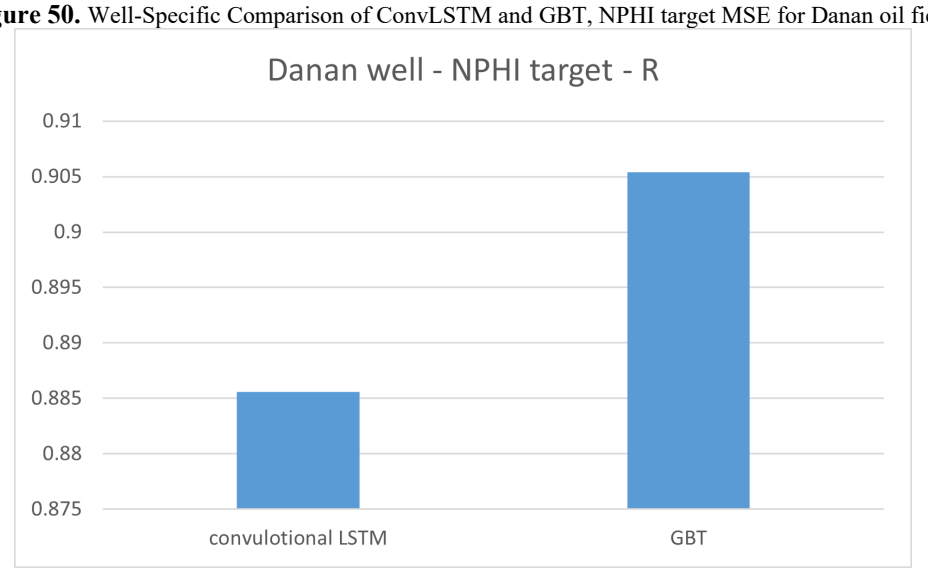

Figure 51. Well-Specific Comparison of ConvLSTM and GBT, NPHI target R for Danan oil field.

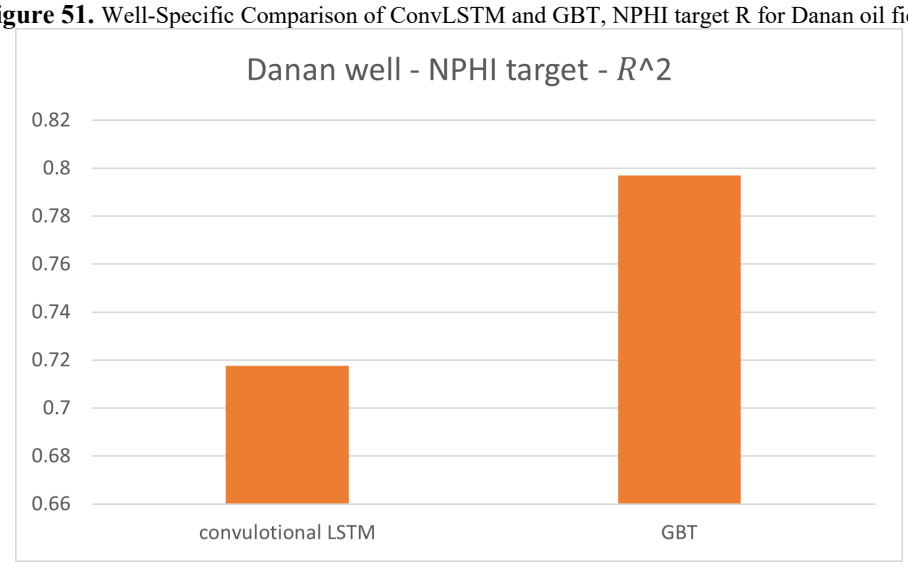

Figure 52. Well-Specific Comparison of ConvLSTM and GBT, NPHI target R^2 for Danan oil field.

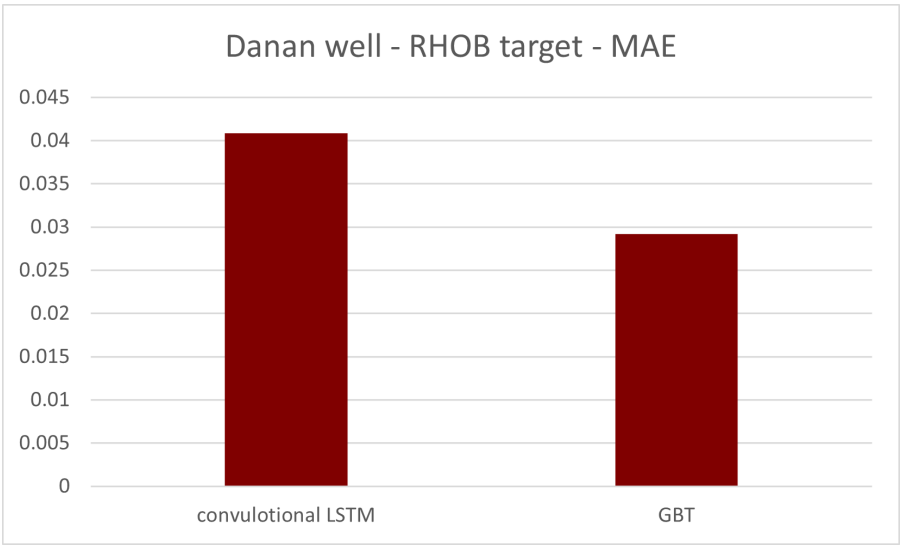

Figure 53. Well-Specific Comparison of ConvLSTM and GBT, RHOB target MAE for Danan oil field.

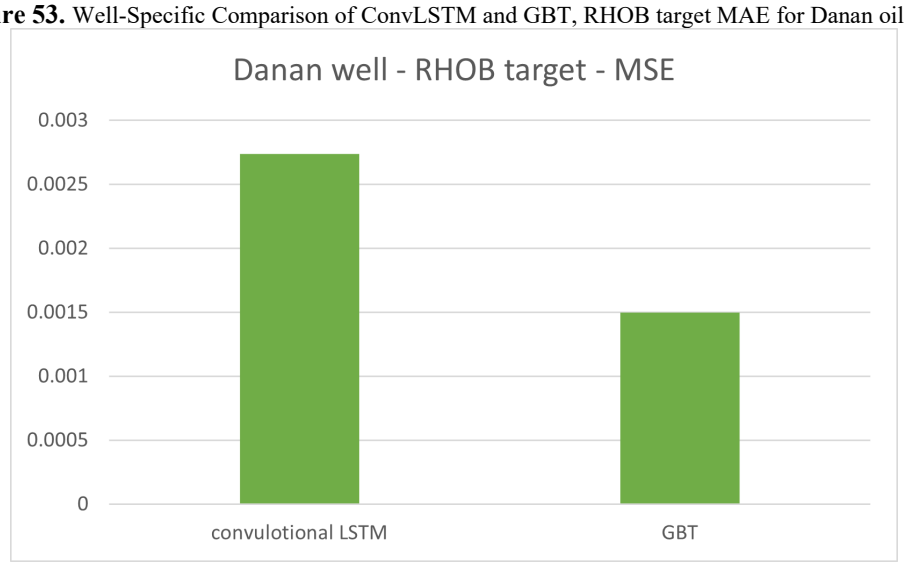

Figure 54. Well-Specific Comparison of ConvLSTM and GBT, RHOB target MSE for Danan oil field.

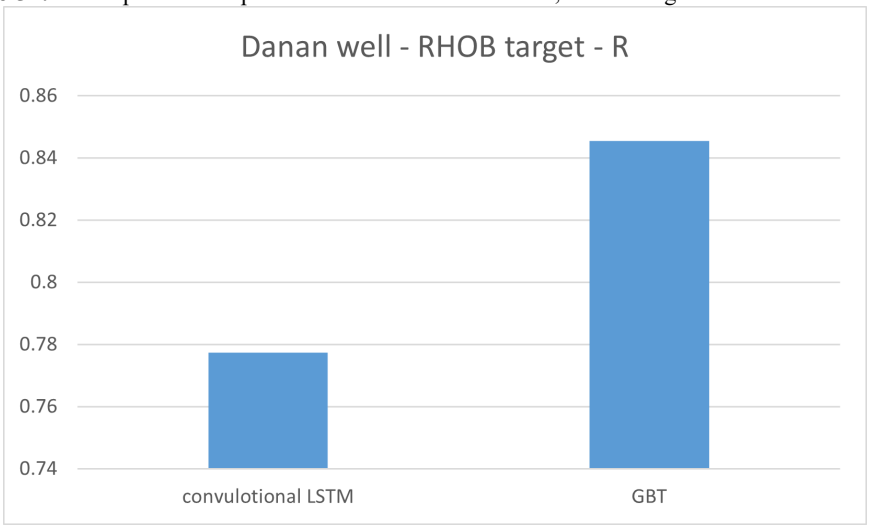

Figure 55. Well-Specific Comparison of ConvLSTM and GBT, RHOB target R for Danan oil field.

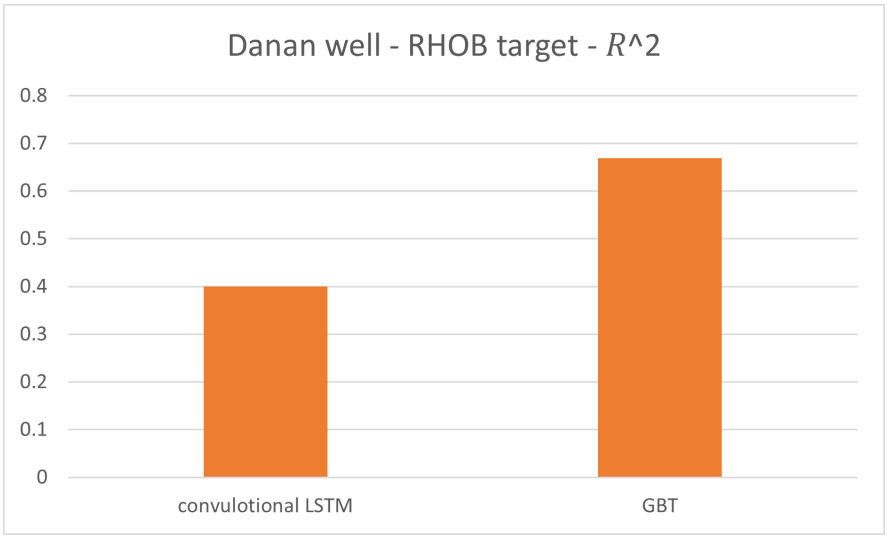

Figure 56. Well-Specific Comparison of ConvLSTM and GBT, RHOB target R^2 for Danan oil field.

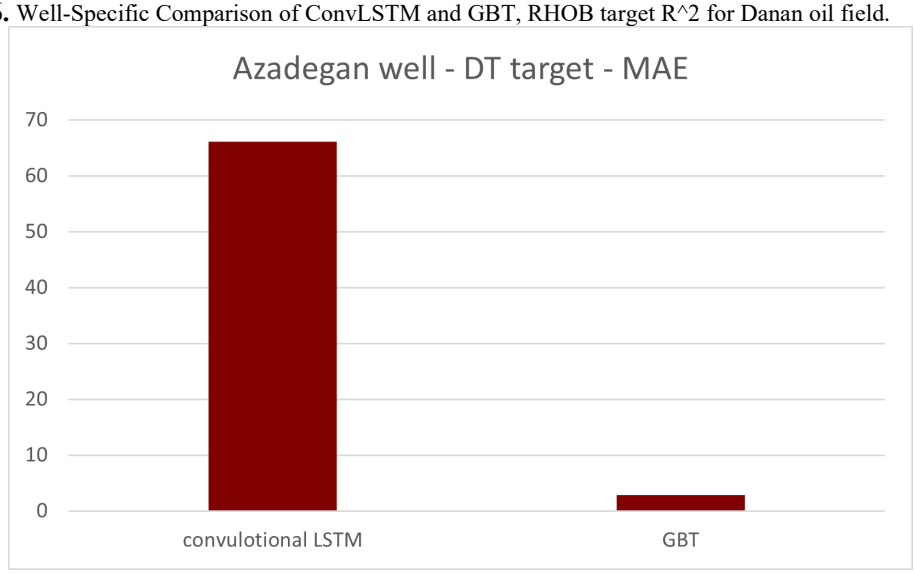

Figure 57. Well-Specific Comparison of ConvLSTM and GBT, MAE target DT for Azadegan oil field.

Figure 58. Well-Specific Comparison of ConvLSTM and GBT, MSE target DT for Azadegan oil field.

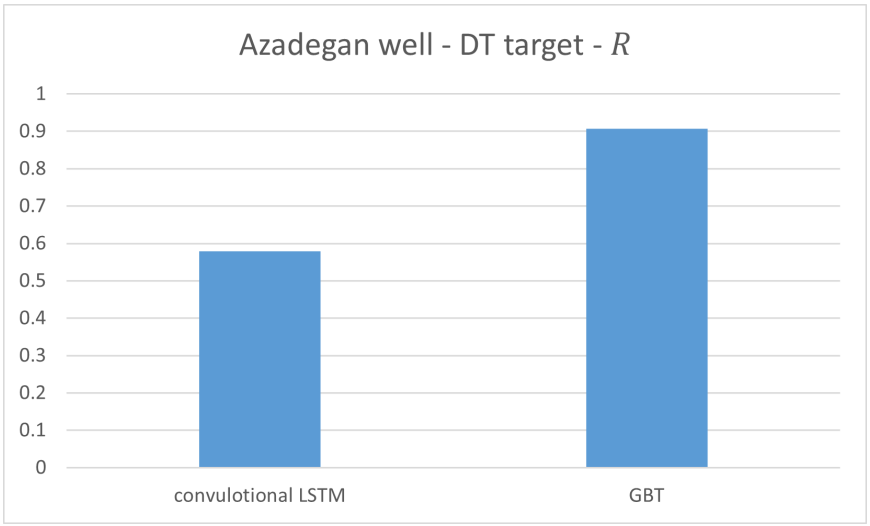

Figure 59. Well-Specific Comparison of ConvLSTM and GBT, R target DT for Azadegan oil field.

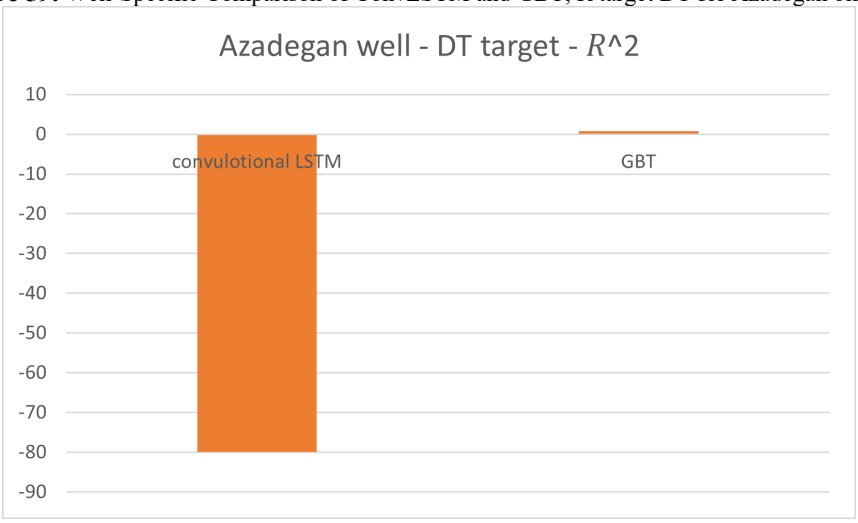

Figure 60. Well-Specific Comparison of ConvLSTM and GBT, R^2 target DT for Azadegan oil field.

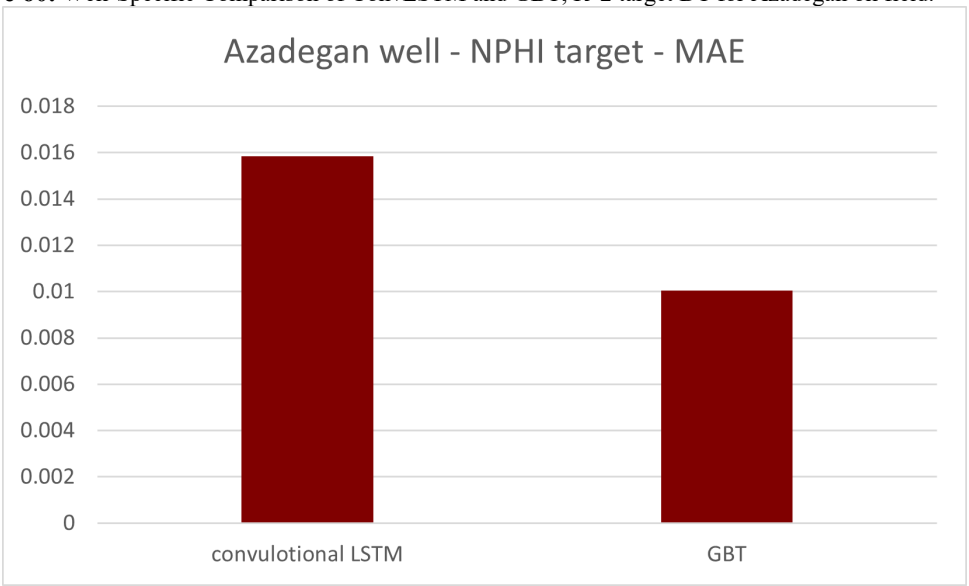

Figure 61. Well-Specific Comparison of ConvLSTM and GBT, NPHI target MAE for Azadegan oil field.

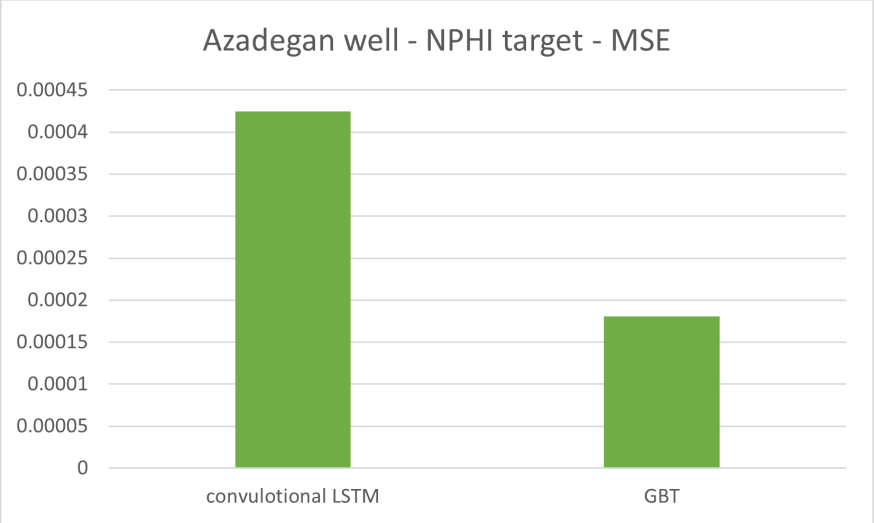

Figure 62. Well-Specific Comparison of ConvLSTM and GBT, NPHI target MSE for Azadegan oil field.

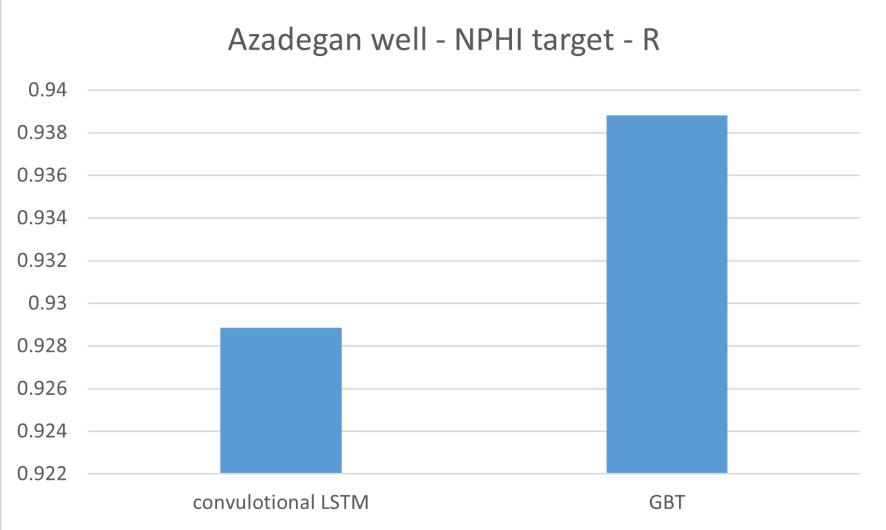

Figure 63. Well-Specific Comparison of ConvLSTM and GBT, NPHI target R for Azadegan oil field.

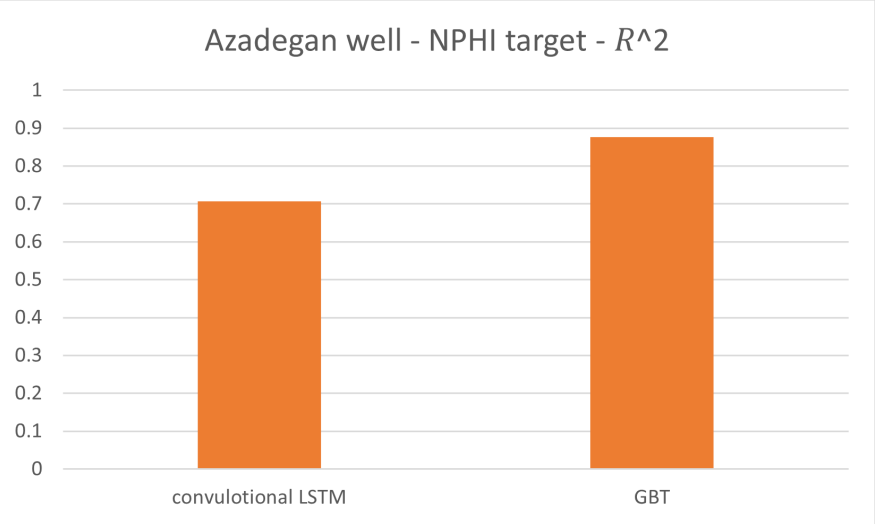

Figure 64. Well-Specific Comparison of ConvLSTM and GBT, NPHI target R^2 for Azadegan oil field.

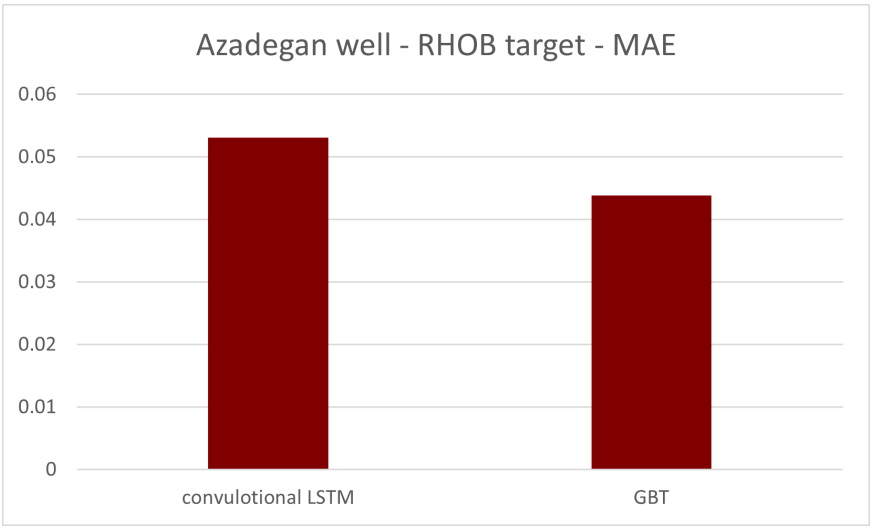

Figure 65. Well-Specific Comparison of ConvLSTM and GBT, RHOB target MAE for Azadegan oil field.

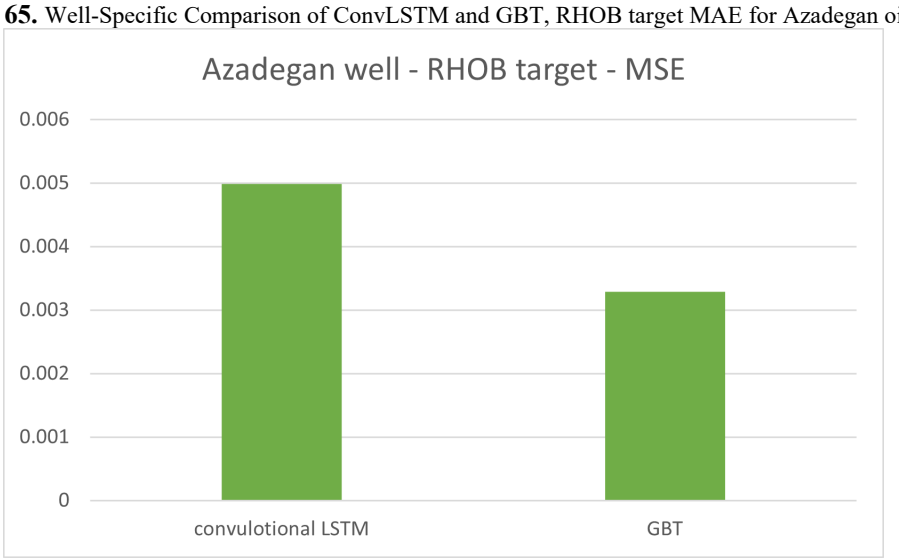

Figure 66. Well-Specific Comparison of ConvLSTM and GBT, RHOB target MSE for Azadegan oil field.

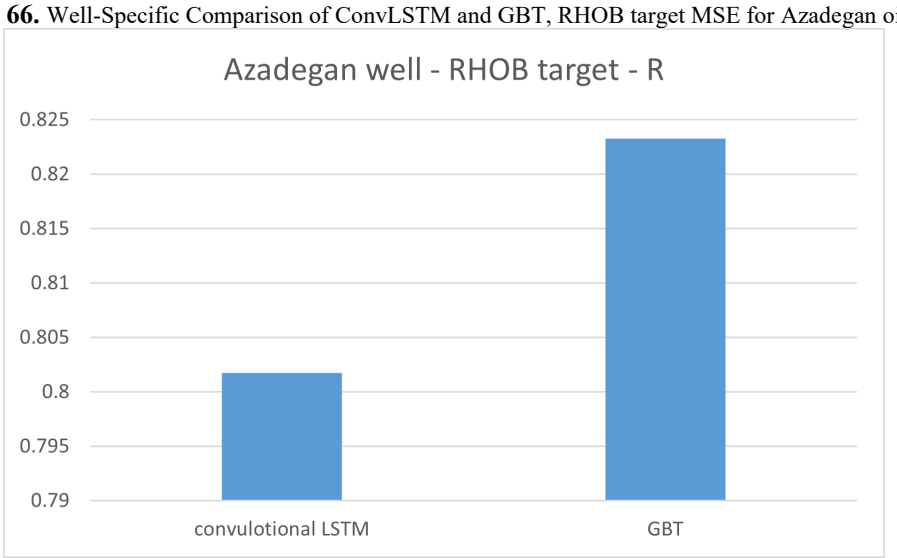

Figure 67. Well-Specific Comparison of ConvLSTM and GBT, RHOB target R for Azadegan oil field.

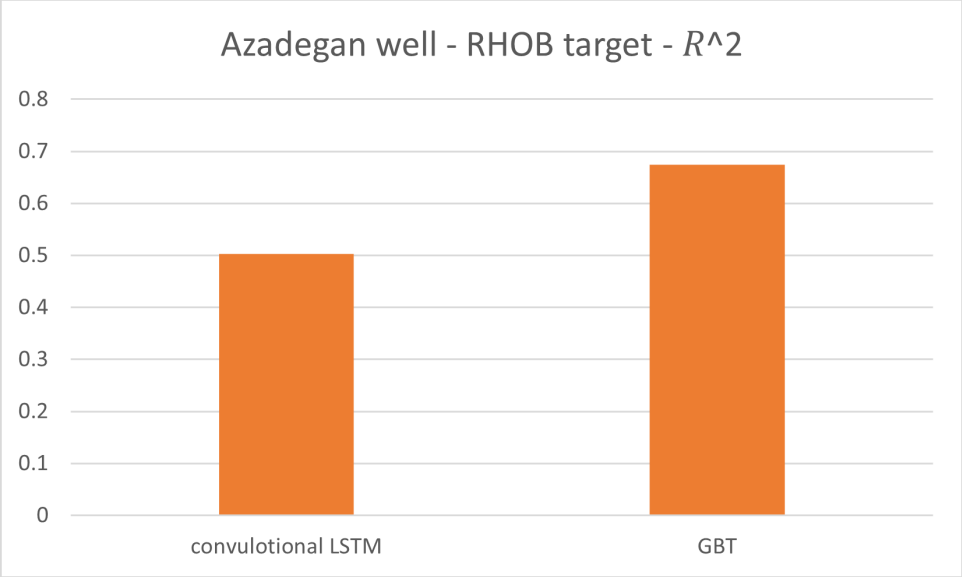

Figure 68. Well-Specific Comparison of ConvLSTM and GBT, RHOB target R^2 for Azadegan oil field.

4.6 Cross-Field Comparative Analysis: Azadegan vs. Danan

To assess the influence of reservoir heterogeneity on model performance, a cross-field comparative analysis was conducted between the Azadegan and Danan fields. Although both fields belong to the Sarvak Formation, their petrophysical behavior differs considerably, reflecting distinct degrees of lithological variability, diagenetic alteration, and borehole stability.

4.6.1 Geological and Log-Variability Differences.

The Azadegan field exhibits higher heterogeneity characterized by abrupt facies transitions, localized vuggy porosity, and frequent borehole enlargement. These conditions produce higher variance in DT and NPHI, along with stronger non-stationary depth trends. The Danan field, in contrast, displays more uniform porosity–density relationships and smoother depth-dependent patterns. These differences are reflected in the feature-importance plots (Figures 3-8), where Azadegan shows stronger depth dependence and greater feature imbalance for DT, whereas Danan presents more evenly distributed predictor contributions.

4.6.2 Model-Performance Implications.

The heterogeneity contrast between the fields explains several observed modeling trends. GBT yielded consistent performance in both fields, but its relative advantage was most pronounced in Azadegan, where nonlinear and irregular relationships were more challenging for ConvLSTM to capture. In Danan, ConvLSTM maintained reasonable accuracy for NPHI and RHOB due to the smoother sequential structure of the logs. However, in Azadegan, ConvLSTM exhibited wider error distributions, greater divergence in DT prediction, and expanded uncertainty intervals, particularly in intervals containing facies transitions or borehole instability.

4.6.3 Role of Heterogeneity in DT Prediction.

The DT target showed the strongest

cross-field contrast. In Azadegan, DT displayed high-frequency variability and strong depth-dominant behavior, which interfered with ConvLSTM's sequential-learning assumptions. In Danan, DT retained some continuity, enabling more stable training but still lagging behind GBT. These patterns indicate that heterogeneity amplifies ConvLSTM instability while exerting limited impact on the hierarchical partitioning mechanism of GBT.

Overall, the cross-field comparison highlights that reservoir heterogeneity significantly influences model behavior: GBT remains robust under both geological settings, whereas ConvLSTM is sensitive to noise and stratigraphic variability, particularly in highly heterogeneous fields such as Azadegan.

4.7 Feature-Importance - Based Model Behavior Analysis

To explain the observed performance differences between the ensemble-based GBT workflow and the ConvLSTM architecture, a feature-importance analysis was performed for all prediction targets (NPHI, RHOB, and DT) in both the Danan and Azadegan fields. The corresponding feature-importance plots are shown in Figures (Figures 3-8). These results reveal that the contrasting behavior of the two models is fundamentally data-driven and directly linked to the statistical structure and heterogeneity of each target log.

4.7.1 NPHI Prediction Behavior

Across both fields, NPHI exhibits a balanced and geologically coherent dependency on RHOB, WELL_en, RD, and DEPTH (see Figures 3 and 7). In the Azadegan field, RHOB, WELL_en, and DEPTH collectively dominate the predictive structure (importance values between 400–600), while in Danan a similar stable pattern is observed. These predictors are low-noise and smoothly varying, forming depth-consistent relationships. Consequently, ConvLSTM is able to leverage sequential patterns effectively, resulting in competitive performance with GBT for NPHI.

4.7.2 RHOB prediction behavior

Feature-importance patterns for RHOB (shown in Figures 5 and 8) indicate moderate dependency on DEPTH, resistivity, gamma-ray logs, and NPHI, with no single feature overwhelmingly dominant. This multi-source structure favors tree-based models, which can extract local interactions without assuming sequential continuity. ConvLSTM performs reasonably well for RHOB but consistently below GBT, reflecting its difficulty in capturing unaligned multi-feature interactions compared to GBT's hierarchical partitioning.

4.7.3 DT prediction behavior and source of instability

DT exhibits a dramatically different feature-importance profile in both oil fields, clearly visible in Figures 5 and 8. DT depends overwhelmingly on DEPTH (≈680–750 importance units), far exceeding all other logs. However, unlike NPHI, this DEPTH dependency is highly non-stationary: DT contains abrupt vertical changes related to fractures, vugs, lithological transitions, and borehole-condition noise. Additional predictors such as RD, GR, RHOB, and NPHI contribute meaningfully but do not stabilize the inherent irregularity of the DT signal.

The above characteristics explain why ConvLSTM, which assumes locally consistent depth patterns, becomes unstable

for DT and produces large error magnitudes or divergence. GBT, by contrast, does not rely on sequential coherence and can isolate abrupt shifts using decision-tree splits, yielding consistently stable DT predictions in both fields. Overall, the feature-importance results (Figures 3 to 8) demonstrate that the superior robustness of GBT is directly tied to the statistical profile of each target log, while the strengths and limitations of ConvLSTM arise from its sequential modeling assumptions and sensitivity to noise.

4.8 Summary of results

In brief, the MICE+GBT workflow yielded accurate, robust, and interpretable predictions, demonstrating particular excellence in DT log reconstruction where ConvLSTM faltered. The ConvLSTM architecture captured local patterns effectively for NPHI but proved susceptible to noise and constrained by dataset size, resulting in broader error distributions. Collectively, the visualizations including depth-wise profiles, scatter plots, error histograms, and well-specific bar charts underscore that, while deep learning architectures offer considerable potential, ensemble approaches presently afford more reliable solutions for heterogeneous carbonate reservoirs with limited training data. In addition, the feature-importance plots confirmed that the inconsistent performance of ConvLSTM is directly linked to target-specific data characteristics, with NPHI exhibiting stable depth-dependent features conducive to sequence learning, whereas DT displays highly irregular, noise-dominated behavior that is better captured by the tree-based structure of GBT.

Table 2. The results of targeted logs and used models including R, R^2, MSE, and MAE.

Test Well	Target log	model	R	R^2	MSE	MAE
Danan	RHOB	GBT	0.8454	0.6693	0.001498	0.02922
		convolutional LSTM	0.7773	0.3998	0.002739	0.040858
	NPHI	GBT	0.9053	0.7970	0.000234	0.012060
		convolutional LSTM	0.8855	0.7175	0.000329	0.014144
	DT	GBT	0.9022	0.7394	3.54366	1.526272
		convolutional LSTM	-0.7790	-195.8036	2667.39354	51.472448
Azadegan	RHOB	GBT	0.8232	0.6740	0.003288	0.043858
		convolutional LSTM	0.8017	0.5031	0.004984	0.05313
	NPHI	GBT	0.9388	0.8769	0.000180	0.010033
		convolutional LSTM	0.9288	0.7065	0.000425	0.015839
	DT	GBT	0.9076	0.7644	12.958447	2.840505
		convolutional LSTM	0.5786	-79.8470	4419.713264	66.077359

4.9 Computational efficiency and deployment considerations

To ensure a fair comparison, both the ConvLSTM and MICE+GBT workflows were executed under identical hardware and software settings. Empirical tests showed that ConvLSTM required approximately 55–65 minutes per training run due to its recurrent structure and iterative optimization, whereas the complete MICE+GBT cycle (imputation plus training) required only 4–6 minutes. Even if additional computational resources were allocated to accelerate ConvLSTM training, the ensemble-based workflow remained superior in both accuracy and runtime efficiency, making it more suitable for practical deployment in operational reservoir studies.

5 Conclusion

This study presented a comparative evaluation of statistical-ensemble (MICE+GBT) and deep learning (ConvLSTM) approaches for reconstructing missing well logs in the heterogeneous carbonate reservoir from Sarvak Formation. By targeting key petrophysical parameters NPHI, RHOB, and DT under realistic missingness scenarios, the analysis highlighted important methodological trade-offs. Results demonstrated that the MICE+GBT workflow consistently delivered accurate, stable, and interpretable predictions across both Danan and Azadegan fields. Its strength was most evident in DT reconstruction, where ConvLSTM struggled with convergence and produced elevated error magnitudes. Ensemble models also yielded narrower error distributions and superior generalization across wells, underscoring their robustness in data-limited carbonate environments. Conversely, the ConvLSTM framework captured local depth-wise dependencies effectively, particularly for NPHI, and showed potential when sufficient training data were available. However, its sensitivity to heterogeneity and tendency toward error dispersion limit its reliability in reservoirs with strong lithological variability. Overall, the findings suggest that ensemble methods presently offer more dependable solutions for carbonate reservoirs with restricted datasets, while deep learning approaches hold promise for future applications given larger, more diverse training corpora. Integrating the interpretability and stability of ensemble models with the representational power of deep learning could form the basis of next-generation workflows for missing log prediction. This work advances practical methodologies for subsurface characterization in complex reservoirs and provides a benchmark for future research. Extensions of this study could include testing hybrid ensemble–DL architectures, incorporating seismic or core data for improved constraints, and exploring transformer-based models for capturing long-range dependencies more efficiently.

NOMENCLATURE

Nomenclature	
BI	Bit size
CALI	Caliper log
CNN	Convolutional Neural Network
ConvLSTM	Convolutional Long Short-Term Memory
CGR	Corrected Gamma Ray
DT	Compressional sonic travel time (μs/ft)
DRHO	Density correction log
GBT	Gradient Boosted Trees
GR	Gamma Ray
LSTM	Long Short-Term Memory
MAE	Mean Absolute Error
MICE	Multivariate Imputation by Chained Equations
ML	Machine Learning
MSE	Mean Squared Error
MWLT	Missing Well Log Prediction
NPHI	Neutron Porosity (v/v)
PEF	Photoelectric Factor (barns/electron)
RD	Deep Resistivity ($\log_{10}$ scale)
RHOB	Bulk Density (g/cm³)
R	Correlation Coefficient
R^2	Coefficient of Determination

Acknowledgment
We are profoundly grateful for the enduring financial and data support of Asmary field services company.

References

Hu, Wenyi, and Brian W. Horn. "Fourth International Meeting for Applied Geoscience & Energy." . ISSN (Online): 1949-4645. (2024)

Artun, E., et al. "An Integrated Workflow for Data Analytics-Assisted Reservoir Management with Incomplete Well Log Data." *SPE Journal* 30.02 (2025): 486-506.

Mukherjee, Bappa, Kalachand Sain, and Xinming Wu. "Missing log prediction using machine learning perspectives: A case study from upper Assam basin." *Earth Science Informatics* 17.4 (2024): 3071-3093.

Al-Mudhafar, Watheq J., et al. "Machine learning with hyperparameter optimization applied in facies-supported permeability modeling in carbonate oil reservoirs." *Scientific Reports* 15.1 (2025): 12939.

Maldonado-Cruz, Eduardo, John T. Foster, and Michael J. Pyrcz. "Sonic well-log imputation through machine-learning-based uncertainty models." *Petrophysics* 64.02 (2023): 253-270.

Gardner, G. H. F., L. W. Gardner, and ARw Gregory. "Formation velocity and density—The diagnostic basics for stratigraphic traps." *Geophysics* 39.6 (1974): 770-780.

Castagna, John P., Michael L. Batzle, and Raymond L. Eastwood. "Relationships between compressional-wave and shear-wave velocities in clastic silicate rocks." *geophysics* 50.4 (1985): 571-581.

Lopes, Rui L., and Alípio M. Jorge. "Assessment of predictive learning methods for the completion of gaps in well log data." *Journal of Petroleum Science and Engineering* 162 (2018): 873-886.

Pham, N., and E. Zabihi Naeini. "Missing well log prediction using deep recurrent neural networks." *81st EAGE Conference and Exhibition 2019*. Vol. 2019. No. 1. European Association of Geoscientists & Engineers, 2019.

Shan, Liqun, et al. "CNN-BiLSTM hybrid neural networks with attention mechanism for well log prediction." *Journal of Petroleum Science and Engineering* 205 (2021): 108838.

Lin, Lei, et al. "MWLT: Transformer-based missing well log prediction." *Available at SSRN 4236228* (2023).

Lin, Lei, et al. "A deep-learning framework for borehole formation properties prediction using heterogeneous well-logging data: A case study of a carbonate reservoir in the Gaoshiti-Moxi area, Sichuan Basin, China." *Geophysics* 89.1 (2024): WA295-WA308.

Kiss, Viktória, and Norbert Péter Szabó. "Correlation-based imputation method for estimating missing well log data in a Hungarian groundwater well." *MULTIDISZCIPLINÁRIS TUDOMÁNYOK: A MISKOLCI EGYETEM KÖZLEMÉNYE* 12.3 (2022): 89-106.

Alimohammadi, Hamzeh, Saman Mahmoudi, and Shengnan Chen. "Single and multi-well synthetic well log generation using multivariate analysis." *Abu Dhabi International Petroleum Exhibition and Conference*. SPE, 2020.

Kanfar, Rayan, et al. "Real-time well log

prediction from drilling data using deep learning." *arXiv preprint arXiv:2001.10156* (2020).

Hallam, Antony, Debajoy Mukherjee, and Romain Chassagne. "Multivariate imputation via chained equations for elastic well log imputation and prediction." *Applied Computing and Geosciences*. ISSN (Online): 2666-9997. (2022).

Mukherjee, Bappa, et al. "Deep learning-aided simultaneous missing well log prediction in multiple stratigraphic units: a case study from the Bhogpara oil field, Upper Assam, Northeast India." *Earth Science Informatics*. ISSN (Online): 1865-0481. (2024).